Eur. Phys. J. C (2017) 77:12
DOI 10.1140/epjc/s10052-016-4588-5

THE EUROPEAN PHYSICAL JOURNAL C

Regular Article - Theoretical Physics

Decays of B, B_s and B_c to D-wave heavy–light mesons

Qiang Li[a], **Tianhong Wang**[b], **Yue Jiang**[c], **Han Yuan**[d], **Tian Zhou**[e], **Guo-Li Wang**[f]

Harbin Institute of Technology, Harbin 150001, People's Republic of China

Received: 14 November 2016 / Accepted: 20 December 2016 / Published online: 6 January 2017

Abstract We study the weak decays of $\bar{B}_{(s)}$ and B_c into D-wave heavy–light mesons, including $J^P = 2^-$ ($D_{(s)2}$, $D'_{(s)2}$, $B_{(s)2}$, $B'_{(s)2}$) and 3^- ($D^*_{(s)3}$, $B^*_{(s)3}$) states. The weak decay hadronic matrix elements are obtained based on the instantaneous Bethe–Salpeter method. The branching ratios for the $\bar{B}$ decays are $\mathcal{B}[\bar{B} \to D_2 e\bar{\nu}_e] = 1.1^{-0.3}_{+0.3} \times 10^{-3}$, $\mathcal{B}[\bar{B} \to D'_2 e\bar{\nu}_e] = 4.1^{-0.8}_{+0.9} \times 10^{-4}$, and $\mathcal{B}[\bar{B} \to D^*_3 e\bar{\nu}_e] = 1.0^{-0.2}_{+0.2} \times 10^{-3}$, respectively. For the semi-electronic decays of $\bar{B}_s$ to D_{s2}, D'_{s2}, and D^*_{s3}, the corresponding branching ratios are $1.7^{-0.5}_{+0.5} \times 10^{-3}$, $5.2^{-1.5}_{+1.6} \times 10^{-4}$, and $1.5^{-0.4}_{+0.4} \times 10^{-3}$, respectively. The branching ratios of the semi-electronic decays of B_c to D-wave D mesons are in the order of 10^{-5}. We also obtained the forward–backward asymmetry, angular spectra, and lepton momentum spectra. In particular the distribution of decay widths for the 2^- states D_2 and D'_2 varying along with mixing angle are presented.

1 Introduction

The D-wave $D_{(s)}$ mesons have attracted lots of attention since numerous excited charmed states are discovered by BaBar [1], and LHCb [2–5]. In 2010 BaBar observed four signals $D(2550)^0$, $D^*(2600)^0$, $D(2750)^0$, and $D^*(2760)^0$ for the first time [1], where the last two are expected to lie in the mass region of four D-wave charm mesons [6]. Later the LHCb reported two natural parity resonances $D^*_J(2650)^0$ and $D^*_J(2760)^0$ in the $D^{*+}\pi^-$ mass spectrum and measured their angular distribution [2]. The same final states also show the presence of two unnatural parity states, $D_J(2580)^0$ and $D_J(2740)^0$. Here the natural parity denotes states with $J^P = 0^+, 1^-, 2^+, 3^-, \ldots$ with $P = (-1)^J$, while the unnatural parity indicates series with $J^P = 0^-, 1^+, 2^-, \ldots$.

Then in May 2015, LHCb confirmed that the $D^*_J(2760)^0$ resonance has spin 1 [4]. The mass and width are measured as $m[D^*_1(2760)^0] = 2781 \pm 22$ MeV and $\Gamma[D^*_1(2760)^0] = 177 \pm 38$ MeV, where we have combined the statistical and systematic uncertainties in quadrature for simplicity. Later LHCb determined $D^*_J(2760)^-$ to have spin–parity 3^- and it is interpreted as $D^*_3(2760)^-$, namely the ${}^3D_3$ $\bar{c}d$ state. The mass and width are measured as $m[D^*_3(2760)] = 2798 \pm 10$ MeV and $\Gamma[D^*_3(2760)] = 105 \pm 30$ MeV [5].

For the D-wave charm–strange meson, BarBar first observed the $D^*_{sJ}(2860)$ [7,8]. And then LHCb's results support the idea that $D^*_{sJ}(2860)$ is an admixture of the spin-1 and spin-3 [3,9]. The measured mass and width for D^*_{s3} are 2861 ± 7 and 53 ± 10 MeV, respectively. The two D-wave charm–strange mesons with $J = 2$, namely the 2^- states D_{s2} and D'_{s2}, are still undiscovered in experiment.

The identification of these new excited charmed mesons can be found in Refs. [10–20]. We will follow Godfrey's assignments on D-wave $D^{(*)}_{(s)J}$ mesons in Ref. [20], where $D^*_{s3}(2860)$ is identified as 1^3D_3 $c\bar{s}$; $D^*_3(2798)^0$ is identified as $1^3D_3(c\bar{q})$ state; $D^*_1(2760)^0$ is interpreted as $1^3D_1(c\bar{q})$; and the $D_J(2750)^0$ reported by BaBar and $D_J(2740)^0$ reported by LHCb are identified as the same state with $1D_2(c\bar{q})$, where q denotes a light quark u or d.

These D-wave excited states still need more experimental data to be discovered or confirmed. The identification and spin–parity assignments in the above literature are just tentative. As the LHC accumulates more and more data, the study of these D-wave charm and charm–strange mesons in the weak decay of $B_{(s)}$ and B_c meson becomes necessary and important. The properties of $D^{(*)}_{(s)J}$ in $B_{(s)}$ and B_c decays would be helpful in identification of these excited $D_{(s)}$ mesons. The semi-leptonic decays of $B_{(s)}$ into D-wave charmed mesons have been studied by QCD sum rules [21–23] and constituent quark models in the framework of heavy

[a] e-mail: lrhit@protonmail.com
[b] e-mail: thwang@hit.edu.cn
[c] e-mail: jiangure@hit.edu.cn
[d] e-mail: hanyuan@hit.edu.cn
[e] e-mail: tianzhou@hit.edu.cn
[f] e-mail: gl_wang@hit.edu.cn

quark effective theory (HQET) [24,25]. Most of previous work is based on the HQET. The systematic studies on weak decays of $\bar{B}_{(s)}$ into D-wave $D_{(s)2}$, $D'_{(s)2}$ and $D^*_{(s)3}$ are still quite less while all these D-wave charmed mesons can hopefully be detected in the near future experiments. On the other hand, in 2012 the BaBar Collaboration reported the ratio of $\mathcal{B}(\bar{B} \to D^{(*)}\tau^-\bar{\nu}_\tau)$ relative to $\mathcal{B}(\bar{B} \to D^{(*)}e^-\bar{\nu}_e)$, which exceed the standard model expectation by 2σ (2.7σ) [26] and may hint the new physics. We also noticed that in the very recently Belle measurement [27], the experimental results on this quantity are consistent with the theoretical predictions [28–30] in the framework of the Standard Model. Anyway, it is still necessary and helpful to investigate these ratios for the $\bar{B}_{(s)}$ and B_c decays into higher excited $D_{(s)}$ mesons.

In this work we will concentrate on the semi-leptonic and non-leptonic decays of $\bar{B}$ ($\bar{B}_s$, B_c) into D-wave D (D_s) meson, including 2^- ($D_{(s)2}$, $D'_{(s)2}$) and 3^- ($D^*_{(s)3}$) states. For completeness, the weak decays of B_c to D-wave bottomed mesons are also studied. We use the Instantaneous Bethe–Salpeter equation (IBS) [31] to get the hadronic transition form factors. The BS equation [32] is the relativistic two-body bound states formula. Based on our previous studies [33–36], the relativistic corrections for transitions of higher excited states are larger and more important than that for the ground states, so the relativistic method is more reliable for the processes involved the high excited states. In the instantaneous approximation of the interaction kernel, we can obtain the Salpeter equation. The Salpeter method has been widely used to deal with heavy mesons' decay constants calculation [37,38], annihilation rate [39,40], and hadronic transition [33–36].

This paper is organized as follows: first we present the general formalism of semi-leptonic and non-leptonic decay for the $\bar{B}_{(s)}$ meson, including decay width, forward–backward asymmetry, and lepton spectra. In Sect. 3 we compute the form factors in hadronic transition by the Salpeter method. In Sect. 4 we give the numerical results and discussions. Finally we give a short summary of this work.

2 Formalism of semi-leptonic and non-leptonic decays

In this section, firstly we will derive the formalism of transition amplitudes for the $\bar{B}_{(s)}$ to D-wave heavy–light mesons. Then the formalisms of interested observables are presented. We will take the $\bar{B} \to D_J^{(*)}$ transition as an example to show the calculation details, while results for the transition of B_s and B_c will be given directly.

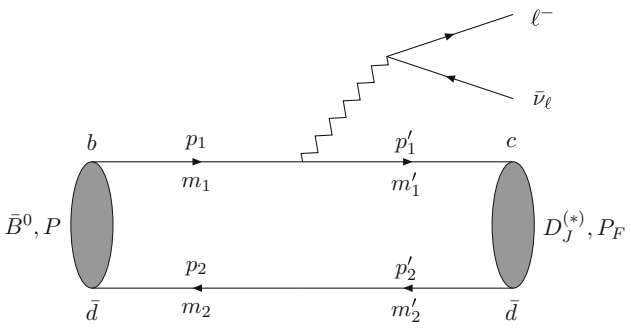

Fig. 1 Feynman diagram for semi-leptonic decay of $\bar{B}$ to $D_J^{(*)}$ ($J = 2, 3$). $m_i\,(m'_i)$ and $p_i\,(p'_i)$ are the constituent quark mass and momentum for initial (final) state, respectively

2.1 Semi-leptonic decay amplitude

The Feynman diagram responsible for $\bar{B}$ semi-leptonic decay is showed in Fig. 1, where we use P and P_F to denote the momenta of $\bar{B}$ and $D_J^{(*)}$, respectively.

The transition amplitude $\mathcal{A}$ for the process $\bar{B} \to D_J^{(*)}\ell\bar{\nu}$ can be written directly as

$$\mathcal{A} = \frac{G_F}{\sqrt{2}} V_{cb} l^\mu \langle D_J^{(*)}|J_\mu|\bar{B}\rangle. \tag{1}$$

In the above equation, G_F denotes the Fermi weak coupling constant; V_{cb} is the Cabibbo–Kobayashi–Maskawa matrix element; the lepton matrix element l^μ reads

$$l^\mu = \bar{u}(p_\ell)\Gamma^\mu v(p_\nu), \tag{2}$$

where ℓ ($\bar{\nu}_\ell$) denotes the charged lepton (anti-neutrino), and $p_\ell(p_\nu)$ denotes the corresponding momentum, and the definition $\Gamma^\mu = \gamma^\mu(1-\gamma^5)$ is used; $\langle D_J^{(*)}|J_\mu|\bar{B}\rangle$ is the hadronic transition element, where $J_\mu = \bar{c}\Gamma_\mu b$ is the weak current.

We use $\mathcal{M}^\mu$ to denote the hadronic transition element $\langle D_J^{(*)}|J^\mu|\bar{B}\rangle$, which can be described with form factors. The general form of the hadronic matrix element depends on the total angular momentum J of the final meson. For D_2 (D'_2) and D^*_3 the form factors are defined as

$$\mathcal{M}^\mu = \begin{cases} e_{\alpha\beta}P^\alpha(s_1P^\beta P^\mu + s_2P^\beta P_F^\mu + s_3g^{\beta\mu} + \mathrm{i}s_4\epsilon^{\mu\beta PP_F}) & \text{if } J=2, \\ e_{\alpha\beta\gamma}P^\alpha P^\beta(h_1P^\gamma P^\mu + h_2P^\gamma P_F^\mu + h_3g^{\gamma\mu} + \mathrm{i}h_4\epsilon^{\mu\gamma PP_F}) & \text{if } J=3. \end{cases} \tag{3}$$

In the above equation, we used the definition $\epsilon_{\mu\nu PP_F} = \epsilon_{\mu\nu\alpha\beta}P^\alpha P_F^\beta$ where $\epsilon_{\mu\nu\alpha\beta}$ is the totally antisymmetric Levi-Civita tensor; $g^{\mu\nu}$ is the Minkowski metric tensor; $e_{\alpha\beta}$ and $e_{\alpha\beta\gamma}$ are the polarization tensor for the $J = 2$ and 3 mesons, respectively, which are completely symmetric; s_i and h_i ($i = 1, 2, 3, 4$) are the form factors for $J = 2$ and 3, respectively. To state it more clearly, we will use s_i, t_i, and h_i to denote the form factors for transitions $\bar{B}$ to D_2, D'_2, and

D_3^*, respectively. S_i, T_i, and H_i are used to represent the form factors of B_c^- to $\bar{D}_2$, D_2', and D_3^*, respectively. The definition forms are the same as that for the transition $\bar{B} \to D_J^{(*)}$, just s_i is replaced by S_i, t_i by T_i, and h_i by H_i. For $\bar{B}_s$ decays, the corresponding form factor behaviors are very similar to $\bar{B}$ decays. The detailed calculations of these form factors will be given in next section.

After summing the polarization of all the final states, including the charged lepton, anti-neutrino and the final $D_J^{(*)}$, we obtain

$$\overline{|\mathcal{A}|^2} = \frac{G_F^2}{2}|V_{cb}|^2 L^{\mu\nu} H_{\mu\nu}, \tag{4}$$

where the lepton tensor $L^{\mu\nu}$ has the following form:

$$L^{\mu\nu} = 8(p_\ell^\mu p_\nu^\nu + p_\nu^\mu p_\ell^\nu - p_\ell \cdot p_\nu g^{\mu\nu} - \mathrm{i}\epsilon^{\mu\nu p_\ell p_\nu}). \tag{5}$$

$H_{\mu\nu}$ is the hadronic tensor describing the propagator-meson interaction vertex, which depends on P, P_F, and the corresponding form factors. It can be written as

$$H_{\mu\nu} = \sum_{s=-J}^{J} \mathcal{M}_\mu^{(s)} \mathcal{M}_\nu^{*(s)} = N_1 P_\mu P_\nu + N_2 (P_\mu P_{F\nu} + P_\nu P_{F\mu}) + N_4 P_{F\mu} P_{F\nu} + N_5 g_{\mu\nu} + \mathrm{i} N_6 \epsilon_{\mu\nu P P_F}, \tag{6}$$

where the summation is over the polarization of the final $D_J^{(*)}$ meson; N_i is related to the form factors s_i for D_2, t_i for D_2' or h_i for D_3^*. The detailed expressions for N_i can be found in Appendix A.

2.2 Non-leptonic decay amplitude

The Feynman diagram for the non-leptonic decay of $\bar{B}$ to $D_J^{(*)}$ and a light meson X is showed in Fig. 2. As a preliminary study for non-leptonic decays of $\bar{B}$ to D-wave D mesons, we will work in the framework of naive factorization approximation [41–44], which has been widely used in heavy mesons' weak decays [45–49]. The factorization assumption is expected to hold for process that involves a heavy meson and a light meson, provided the light meson is energetic [50–52]. Also we only consider the processes when the light meson X is π, ρ, K, or K^*.

In the naive factorization approximation, the decay amplitude can be factorized as the product of two parts, the hadronic transition matrix element and an annihilation matrix element. Then we can write the non-leptonic decay amplitude as

$$\mathcal{A}\big[\bar{B} \to D_J^{(*)} X\big] \simeq \frac{G_F}{\sqrt{2}} V_{cb} V_{uq} a_1(\mu) \langle D_J^{(*)}|J_\mu|\bar{B}\rangle \times \langle X|(\bar{q}u)_{V-A}|0\rangle, \tag{7}$$

where we have used the definition $(\bar{q}u)_{V-A} = \bar{q}\Gamma^\mu u$ and q denotes a d or s quark field; V_{uq} denotes the corresponding

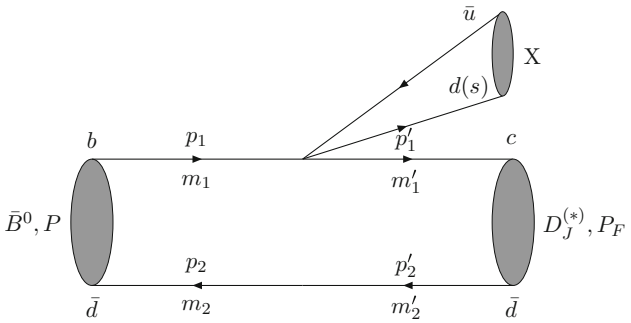

Fig. 2 The Feynman diagram of the non-leptonic decay of $\bar{B}_{(s)}$ meson into D-wave charmed meson. X denotes a light meson

CKM matrix element; $a_1 = c_1 + \frac{1}{N_c} c_2$, where $N_c = 3$ is the number of colors. For b decays, we take $\mu = m_b$, and $a_1 = 1.14$, $a_2 = -0.2$ [47] are used in this work. The annihilation matrix element can be expressed by decay constant as

$$\langle X|(\bar{q}u)_{V-A}|0\rangle = \begin{cases} \mathrm{i} P_X^\mu f_P & X \text{ is a pseudoscalar meson } (\pi, K), \\ e^\mu M_X f_V & X \text{ is a vector meson } (\rho, K^*). \end{cases} \tag{8}$$

M_X, P_X are the mass and momentum of X meson, respectively; the meson polarization vector e^μ satisfies $e_\mu P_X^\mu = 0$ and the completeness relation is given by $\sum_s e_{(s)}^\mu e_{(s)}^\nu = \frac{P_X^\mu P_X^\nu}{M_X^2} - g^{\mu\nu}$, where s denotes the polarization state; f_P and f_V are the corresponding decay constants.

Then $\overline{|\mathcal{A}|^2}$ can be expressed by hadronic tensor $H_{\mu\nu}$, which is just the same as that in the corresponding semi-leptonic decays, and light meson tensor $X^{\mu\nu}$ as

$$\overline{|\mathcal{A}|^2} = \frac{G_F^2}{2}|V_{cb}|^2 |V_{uq}|^2 a_1^2 H_{\mu\nu} X^{\mu\nu}, \tag{9}$$

where $X^{\mu\nu}$ obeys the following expression:

$$X^{\mu\nu} = \langle X|(\bar{q}\Gamma^\mu u)|0\rangle \langle X|\bar{q}\Gamma^\nu u|0\rangle^* = \begin{cases} P_X^\mu P_X^\nu f_P^2 & X \text{ is a pseudoscalar meson}, \\ (P_X^\mu P_X^\nu - M_X^2 g^{\mu\nu}) f_V^2 & X \text{ is a vector meson}. \end{cases} \tag{10}$$

2.3 Several observables

One of the interested quantity in $\bar{B}$ semi-leptonic decay is the angular distribution of the decay width Γ, which can be described as

$$\frac{\mathrm{d}\Gamma}{\mathrm{d}\cos\theta} = \int \frac{1}{(2\pi)^3} \frac{|\boldsymbol{p}_\ell^*||\boldsymbol{p}_F^*|}{16M^3} \overline{|\mathcal{A}|^2} \mathrm{d}m_{\ell\nu}^2, \tag{11}$$

where M is the initial $\bar{B}$ mass; $m_{\ell\nu}^2 = (p_\ell + p_\nu)^2$ is the invariant mass square of ℓ and $\bar{\nu}$; $\boldsymbol{p}_\ell^*$ and $\boldsymbol{p}_F^*$ are the three momenta of ℓ and $D_J^{(*)}$ in the $\ell\bar{\nu}$ rest frame, respectively; θ is

the angle between $\boldsymbol{p}_\ell^*$ and $\boldsymbol{p}_F^*$; $|\boldsymbol{p}_\ell^*| = \frac{1}{2m_{\ell\nu}}\lambda^{\frac{1}{2}}(m_{\ell\nu}^2, M_\ell^2, M_\nu^2)$ and $|\boldsymbol{p}_F^*| = \frac{1}{2m_{\ell\nu}}\lambda^{\frac{1}{2}}(m_{\ell\nu}^2, M^2, M_F^2)$, where we have used the Källén function $\lambda(a,b,c) = (a^2+b^2+c^2-2ab-2bc-2ac)$, M_ℓ and M_ν are the lepton mass and anti-neutrino mass, respectively. Another quantity we are interested is the forward–backward asymmetry $A_{\rm FB}$, which is defined as

$$A_{\rm FB} = \frac{\Gamma_{\cos\theta>0} - \Gamma_{\cos\theta<0}}{\Gamma_{\cos\theta>0} + \Gamma_{\cos\theta<0}}. \tag{12}$$

The decay width varying along with charged lepton 3-momentum $|\boldsymbol{p}_\ell|$ is given by

$$\frac{{\rm d}\Gamma}{{\rm d}|\boldsymbol{p}_\ell|} = \int \frac{1}{(2\pi)^3}\frac{|\boldsymbol{p}_\ell|}{16M^2E_\ell}\overline{|\mathcal{A}|^2}{\rm d}m_{\ell\nu}^2, \tag{13}$$

where E_ℓ denotes the charged lepton energy in the rest frame of the initial state meson.

The non-leptonic decay width of the $\bar{B}$ meson is given by

$$\Gamma = \frac{|\boldsymbol{p}|}{8\pi M^2}\overline{|\mathcal{A}|^2}, \tag{14}$$

where $\boldsymbol{p}$ represents the 3-momentum of the final $D_J^{(*)}$ in $\bar{B}$ rest frame, which is expressed as $|\boldsymbol{p}| = \frac{1}{2M}\lambda^{\frac{1}{2}}(M^2, M_X^2, M_F^2)$.

3 Hadronic transition matrix element

The hadronic transition matrix element $\langle D_J^{(*)}|J^\mu|\bar{B}\rangle$ plays a key role in the calculations of $\bar{B}$ semi-leptonic and non-leptonic decays. In this section we will give details to calculate the hadronic transition matrix element by Bethe–Salpeter method in the framework of constituent quark model.

3.1 Formalism of hadronic transition matrix element with Bethe–Salpeter method

According to the Mandelstam formalism [53], the hadronic transition amplitude $\mathcal{M}^\mu$ can be written by the Beter–Salpeter (BS) wave function as

$$\mathcal{M}^\mu = -{\rm i}\int \frac{{\rm d}^4q{\rm d}^4q'}{(2\pi)^4}{\rm Tr}\big[\bar{\Psi}_D(q', P_F)\Gamma^\mu \times\Psi_B(q, P)(m_2+\not{p}_2)\delta^4(p_2-p_2')\big], \tag{15}$$

where $\Psi_B(q,P)$ and $\Psi_D(q', P_F)$ are the BS wave functions of the $\bar{B}$ meson and the final $D_J^{(*)}$, respectively; $\bar{\Psi}$ is defined as $\gamma^0\Psi^\dagger\gamma^0$; q and q' are, respectively, the inner relative momenta of $\bar{B}$ and $D_J^{(*)}$ system, which are related to the quark (anti-quark) momentum $p_1^{(\prime)}$ ($p_2^{(\prime)}$) by $p_i = \alpha_i P + (-1)^{(i+1)}q$ and $p_i' = \alpha_i' P_F + (-1)^{(i+1)}q'$ $(i = 1,2)$. And here we defined the symbols $\alpha_i = \frac{m_i}{m_1+m_2}$ and $\alpha_i' = \frac{m_i'}{m_1'+m_2'}$, where m_i and m_i' are masses of the constituent quarks in the initial and final bound states, respectively (see Fig. 1). Here in $\bar{B}$ decays we have $m_1 = m_b$, $m_1' = m_c$, $m_2 = m_2' = m_d$. As there is a delta function in the above equation, the relative momenta q and q' are related by $q' = q - (\alpha_2 P - \alpha_2' P_F)$.

In the instantaneous approximation [31], the inner interaction kernel between quark and anti-quark in bound state is independent of the time component $q_P (= q\cdot P)$ of q. By performing the contour integral on q_P and then we can express the hadronic transition amplitude as [36]

$$\mathcal{M}^\mu = \int \frac{{\rm d}^3q_\perp}{(2\pi)^3}{\rm Tr}\left[\frac{\not{P}}{M}\bar{\psi}_D(q_\perp')\Gamma^\mu\psi_B(q_\perp)\right], \tag{16}$$

where we have used the definitions $q_\perp \equiv q - \frac{P\cdot q}{M^2}P$ and $q_\perp' \equiv q' - \frac{P\cdot q'}{M^2}P$. Here ψ denotes the 3-dimensional positive Salpeter wave function (see Appendix B). ψ_B and ψ_D denote the positive Salpeter wave functions for $\bar{B}$ and $D_J^{(*)}$, respectively, and $\bar{\psi}_D$ is defined $\gamma^0\psi_D^\dagger\gamma^0$.

The positive Salpeter wave function for the $^1S_0(0^-)$ state can be written as [54]

$$\psi_B(^1S_0) = \left[A_1 + A_2\frac{\not{P}}{M} + A_3\frac{\not{q}_\perp}{M} + A_4\frac{\not{P}\not{q}_\perp}{M^2}\right]\gamma^5, \tag{17}$$

where we have the following constraint conditions:

$$\begin{aligned} A_1 &= \frac{M}{2}\left[\frac{\omega_1+\omega_2}{m_1+m_2}k_1 + k_2\right], & A_3 &= -\frac{M(\omega_1-\omega_2)}{m_1\omega_2+m_2\omega_1}A_1,\\ A_2 &= \frac{M}{2}\left[k_1 + \frac{m_1+m_2}{\omega_1+\omega_2}k_2\right], & A_4 &= -\frac{M(m_1+m_2)}{m_1\omega_2+m_2\omega_1}A_1. \end{aligned} \tag{18}$$

The definition $\omega_i \equiv \sqrt{m_i^2 - q_\perp^2}$ $(i = 1,2)$ is used. The derivation of Eqs. (17) and (18) can be found in Appendix B. So there are only two undetermined wave functions k_1 and k_2 here, which are the functions of $q_\perp$. The positive Salpeter wave function for the $3^-(^3D_3)$ state with unequal mass of quark and anti-quark has the following forms [55]:

$$\begin{aligned} \psi_D(^3D_3) = {} & e_{\mu\nu\alpha}q_\perp'^\nu q_\perp'^\alpha \\ & \times\left[q_\perp'^\mu\left(n_1 + n_2\frac{\not{P}_F}{M_F} + n_3\frac{\not{q}_\perp'}{M_F} + n_4\frac{\not{P}_F\not{q}_\perp'}{M_F^2}\right)\right. \\ & +\gamma^\mu(n_5M_F + n_6\not{P}_F) \\ & \left.+n_7(\gamma^\mu\not{q}' - q'^\mu) + n_8\frac{(\gamma^\mu\not{P}_F\not{q}_\perp' + \not{P}_F q_\perp'^\mu)}{M_F}\right]. \end{aligned} \tag{19}$$

In the above equation n_i $(i = 1, 2, \ldots, 8)$ can be expressed with four wave functions u_i $(i = 3, 4, 5, 6)$ as below:

$$
\begin{aligned}
n_1 &= \frac{[(\omega_1'+\omega_2')(q_\perp'^2 u_3 + M_F^2 u_5) + (m_1'+m_2')(q_\perp'^2 u_4 - M_F^2 u_6)]}{2M_F(m_1'\omega_2' + m_2'\omega_1')},\\
n_2 &= \frac{[(m_1'-m_2')(q_\perp'^2 u_3 + M_F^2 u_5) + (\omega_1'-\omega_2')(q_\perp'^2 u_4 - M_F^2 u_6)]}{2M_F(m_1'\omega_2' + m_2'\omega_1')},\\
n_3 &= \frac{1}{2}\left[u_3 + \frac{m_2'+m_2'}{\omega_1'+\omega_2'}u_4 - \frac{2M_F^2}{m_1'\omega_2'+m_2'\omega_1'}u_6\right],\\
n_4 &= \frac{1}{2}\left[u_4 + \frac{\omega_1'+\omega_2'}{m_1'+m_2'}u_3 - \frac{2M_F^2}{m_1'\omega_2'+m_2'\omega_1'}u_5\right],\\
n_5 &= \frac{1}{2}\left[u_5 - \frac{\omega_1'+\omega_2'}{m_1'+m_2'}u_6\right], \quad n_6 = \frac{1}{2}\left[u_6 - \frac{m_1'+m_2'}{\omega_1'+\omega_2'}u_5\right],\\
n_7 &= \frac{M_F(\omega_1'-\omega_2')}{(m_1'\omega_2'+m_2'\omega_1')}n_5, \qquad n_8 = \frac{M_F(\omega_1'+\omega_2')}{(m_1'\omega_2'+m_2'\omega_1')}n_6.
\end{aligned}
\tag{20}
$$

In the Salpeter positive wave functions ψ_B and ψ_D above, the undetermined wave functions k_1, k_2 for 0^- and u_i $(i = 3, 4, 5, 6)$ for 3^- can be obtained by solving the full Salpeter equations numerically (see Appendix B). The positive Salpeter wave functions for the $^1D_2$ [40] and the $^3D_2$ [55] states can be found in Appendix C. $e^{\mu\nu\alpha}$ is the symmetric polarization tensor for spin-3 and satisfies the following relations [56]:

$$
e^{\mu\nu\alpha} g_{\mu\nu} = 0, \quad e^{\mu\nu\alpha} P_{F\mu} = 0, \tag{21}
$$

$$
\sum_s e^{abc}_{(s)} e^{\mu\nu\alpha}_{(s)} = \frac{1}{6}\Omega_1^{abc;\mu\nu\alpha} - \frac{1}{15}\Omega_2^{abc;\mu\nu\alpha}, \tag{22}
$$

where

$$
\begin{aligned}
\Omega_1^{abc;\mu\nu\alpha} &= g_\perp^{a\mu} g_\perp^{b\nu} g_\perp^{c\alpha} + g_\perp^{a\mu} g_\perp^{b\alpha} g_\perp^{c\nu} + g_\perp^{a\nu} g_\perp^{b\mu} g_\perp^{c\alpha}\\
&\quad + g_\perp^{a\nu} g_\perp^{b\alpha} g_\perp^{c\mu} + g_\perp^{a\alpha} g_\perp^{b\mu} g_\perp^{c\nu} + g_\perp^{a\alpha} g_\perp^{b\nu} g_\perp^{c\mu},\\
\Omega_2^{abc;\mu\nu\alpha} &= g_\perp^{ab} g_\perp^{c\mu} g_\perp^{\nu\alpha} + g_\perp^{ab} g_\perp^{c\nu} g_\perp^{\mu\alpha} + g_\perp^{ab} g_\perp^{c\alpha} g_\perp^{\mu\nu}\\
&\quad + g_\perp^{ac} g_\perp^{b\mu} g_\perp^{\nu\alpha} + g_\perp^{ac} g_\perp^{b\nu} g_\perp^{\mu\alpha} + g_\perp^{ac} g_\perp^{b\alpha} g_\perp^{\mu\nu}\\
&\quad + g_\perp^{bc} g_\perp^{a\mu} g_\perp^{\nu\alpha} + g_\perp^{bc} g_\perp^{a\nu} g_\perp^{\mu\alpha} + g_\perp^{bc} g_\perp^{a\alpha} g_\perp^{\mu\nu}.
\end{aligned}
\tag{23}
$$

We have used the definition $g_\perp^{\mu\nu} = -g^{\mu\nu} + \frac{P_F^\mu P_F^\nu}{M_F^2}$.

Inserting the initial $\bar{B}$ wave function $\psi_B(^1S_0)$ (Eq. (17)) and the final D_3^* wave function $\psi_D(^3D_3)$ (Eq. (19)) into the hadronic transition amplitude Eq. (16), after calculating the trace and performing the integral in Eq. (16) we obtain the form factors h_i for the $\bar{B} \to D_3^*$ transition defined in Eq. (3). When performing the integral over $\boldsymbol{q}$ in the rest frame of the initial meson, the following formulas are used:

$$
\begin{aligned}
&\int \frac{\mathrm{d}^3\boldsymbol{q}}{(2\pi)^3} q_\perp^\mu = C_1 P_{F\perp}^\mu,\\
&\int \frac{\mathrm{d}^3\boldsymbol{q}}{(2\pi)^3} q_\perp^\mu q_\perp^\nu = C_{21} P_{F\perp}^\mu P_{F\perp}^\nu + C_{22} g_T^{\mu\nu},\\
&\int \frac{\mathrm{d}^3\boldsymbol{q}}{(2\pi)^3} q_\perp^\mu q_\perp^\nu q_\perp^\alpha = C_{31} P_{F\perp}^\mu P_{F\perp}^\nu P_{F\perp}^\alpha\\
&\quad + C_{32}(g_T^{\mu\nu} P_{F\perp}^\alpha + g_T^{\mu\alpha} P_{F\perp}^\nu + g_T^{\alpha\nu} P_{F\perp}^\mu),\\
&\int \frac{\mathrm{d}^3\boldsymbol{q}}{(2\pi)^3} q_\perp^\mu q_\perp^\nu q_\perp^\alpha q_\perp^\beta = C_{41} P_{F\perp}^\mu P_{F\perp}^\nu P_{F\perp}^\alpha P_{F\perp}^\beta\\
&\quad + C_{42}(g_T^{\mu\nu} P_{F\perp}^\alpha P_{F\perp}^\beta + g_T^{\mu\alpha} P_{F\perp}^\nu P_{F\perp}^\beta + g_T^{\alpha\nu} P_{F\perp}^\mu P_{F\perp}^\beta\\
&\quad + g_T^{\alpha\beta} P_{F\perp}^\mu P_{F\perp}^\nu + g_T^{\beta\nu} P_{F\perp}^\mu P_{F\perp}^\alpha + g_T^{\beta\mu} P_{F\perp}^\nu P_{F\perp}^\alpha)\\
&\quad + C_{43}(g_T^{\alpha\beta} g_T^{\mu\nu} + g_T^{\alpha\nu} g_T^{\mu\beta} + g_T^{\alpha\mu} g_T^{\beta\nu}),
\end{aligned}
$$

where $g_T^{\mu\nu}$ are defined as $(g^{\mu\nu} - \frac{P^\mu P^\nu}{P^2})$ and $P_{F\perp}^\mu = (P_F^\mu - \frac{P_F\cdot P}{M^2} P^\mu)$. From the above equations we can easily obtain the following expressions of C_i:

$$
\begin{cases}
C_1 = |\boldsymbol{q}|\cos\eta, & C_{21} = \frac{1}{2}|\boldsymbol{q}|^2(3\cos^2\eta - 1),\\
C_{22} = \frac{1}{2}|\boldsymbol{q}|^2(\cos^2\eta - 1), & C_{31} = \frac{1}{2}|\boldsymbol{q}|^3(5\cos^3\eta - 3\cos\eta),\\
C_{32} = \frac{1}{2}|\boldsymbol{q}|^3(\cos^3\eta - \cos\eta), & C_{41} = \frac{1}{8}|\boldsymbol{q}|^4(35\cos^4\eta - 30\cos^2\eta + 3),\\
C_{42} = \frac{1}{8}|\boldsymbol{q}|^4(5\cos^4\eta - 6\cos^2\eta + 1), & C_{43} = \frac{1}{8}|\boldsymbol{q}|^4(\cos^4\eta - 2\cos^2\eta + 1),
\end{cases}
\tag{24}
$$

where η is the angle between $\boldsymbol{q}$ and $\boldsymbol{P}_F$.

The physical 2^- D-wave states D_2 and D_2' are the mixing states of $^3D_2$ and $^1D_2$ states, whose wave functions are what we solve directly from the full Salpeter equations. Here we will follow Refs. [57] and [58], where the mixing form for the D-wave states is defined with the mixing angle α as

$$
\begin{aligned}
|D_2\rangle &= +\cos\alpha\ |^1D_2\rangle + \sin\alpha\ |^3D_2\rangle,\\
|D_2'\rangle &= -\sin\alpha\ |^1D_2\rangle + \cos\alpha\ |^3D_2\rangle.
\end{aligned}
\tag{25}
$$

In the heavy quark limit ($m_Q \to \infty$), the D mesons are described in the $|J, j_\ell\rangle$ basis, where m_Q denotes the heavy quark mass and j_ℓ denotes the total angular momentum of the light quark. The relations between $|J, j_\ell\rangle$ and $|J, S\rangle$ for $L = 2$ are

$$
\begin{bmatrix} |2, 5/2\rangle \\ |2, 3/2\rangle \end{bmatrix} = \frac{1}{\sqrt{5}} \begin{bmatrix} \sqrt{2+1} & \sqrt{2} \\ -\sqrt{2} & \sqrt{2+1} \end{bmatrix} \begin{bmatrix} |^1D_2\rangle \\ |^3D_2\rangle \end{bmatrix}. \tag{26}
$$

Then the mixing angle for $L = 2$ can be expressed as $\alpha = \arctan\sqrt{2/3} = 39.23°$. So in this definition D_2 corresponds to the $|J^P, j_\ell\rangle = |2^-, 5/2\rangle$ state and D_2' corresponds to the $|2^-, 3/2\rangle$ state. In this work the same mixing angle will also

be used for the 2^- states $D_{s2}^{(\prime)}$ and $B_{(s)2}^{(\prime)}$. Here the mixing angle is the ideal case predicted by the HEQT in the limit of $m_Q \to \infty$. The dependence for decay widths varying over the mixing angle can be seen in Eqs. (29) and (30).

The wave functions of the $^1D_2$ and $^3D_2$ states can be obtained by solving the corresponding Salpeter equations directly. Then the amplitude for physical 2^- states can be considered as the mixing of the transition amplitudes for the $^1D_2$ and $^3D_2$ states, namely

$$\begin{aligned}\mathcal{M}^\mu(D_2) &= +\cos\alpha\ \mathcal{M}^\mu(^1D_2) + \sin\alpha\ \mathcal{M}^\mu(^3D_2),\\ \mathcal{M}^\mu(D_2') &= -\sin\alpha\ \mathcal{M}^\mu(^1D_2) + \cos\alpha\ \mathcal{M}^\mu(^3D_2).\end{aligned} \tag{27}$$

By using Eq. (27), replacing the final state's wave function $\psi_D(^3D_3)$ by $\psi_D(^1D_2)$ and $\psi_D(^3D_2)$, and then repeating the above procedures for the $^3D_3$ state, we can get the form factors s_i for D_2 and t_i for D_2' defined in Eq. (3).

3.2 Form factors

To solve the Salpeter equations, in this work we choose the Cornell potential as the inner interaction kernel as before [54], which is a linear scalar potential plus a vector interaction potential,

$$\begin{aligned}V(\boldsymbol{q}) &= (2\pi)^3 V_s(\boldsymbol{q}) + \gamma^0 \otimes \gamma_0 (2\pi)^3 V_v(\boldsymbol{q}),\\ V_s(\boldsymbol{q}) &= -(\frac{\lambda}{\alpha} + V_0)\delta^3(\boldsymbol{q}) + \frac{\lambda}{\pi^2(\boldsymbol{q}^2+\alpha^2)^2},\\ V_v(\boldsymbol{q}) &= -\frac{2\alpha_s(\boldsymbol{q})}{3\pi^2(\boldsymbol{q}^2+\alpha^2)},\ \alpha_s(\boldsymbol{q}) = \frac{12\pi}{27\ln(a+\frac{\boldsymbol{q}^2}{\Lambda_{\rm QCD}^2})}.\end{aligned} \tag{28}$$

In the above equations, the symbol $\otimes$ denotes that the Salpeter wave function is sandwiched between the two γ^0 matrices. The model parameters we used are the same as before [34], which read

$$\begin{aligned} a &= e = 2.7183, & \alpha &= 0.060\ \text{GeV}, & \lambda &= 0.210\ \text{GeV}^2,\\ m_u &= 0.305\ \text{GeV}, & m_d &= 0.311\ \text{GeV}, & m_s &= 0.500\ \text{GeV},\\ m_c &= 1.62\ \text{GeV}, & m_b &= 4.96\ \text{GeV}, & \Lambda_{\rm QCD} &= 0.270\ \text{GeV}.\end{aligned}$$

The free parameter V_0 is fixed by fitting the mass eigenvalue to experimental value.

With the numerical Salpeter wave function we can obtain the form factors.

Here we plot the $\bar{B} \to D_J^{(*)}$ form factors s_i, t_i, and h_i $(i = 1, 2, 3, 4)$ changing with the square of momentum transfer $t^2 = (P - P_F)^2$ in Fig. 3a–c, respectively, where s_3, t_3, and h_3 are divided by $M_{\bar{B}}^2$ in order to keep the dimension consistent. Fig. 3d–f are the distribution of form factors S_i, T_i, and H_i for $B_c^- \to \bar{D}_J^{(*)}$ transitions. Also we divided S_3, T_3, and H_3 by $M_{B_c}^2$ to keep the dimension consistent. From Fig. 3, we can see that in all the range concerned the form factors are quite smooth along with t^2. And for transitions $\bar{B} \to D_J^{(*)}$, the form factors change slowly and almost linearly when t^2 varies from 0 to $(M - M_F)^2$. For transitions $B_c^- \to \bar{D}_J^{(*)}$, the form factors change dramatically over t^2, especially in the range with large momentum transfer.

4 Numerical results and discussions

Firstly we specify the meson mass, lifetime, CKM matrix elements, and decay constants used in this work. For the mass of the $\bar{B}$, $\bar{B}_s$, and B_c mesons we take the values from PDG [59]. We follow the mass predictions and J^P assignments of Ref. [20] for D-wave charm and charm–strange mesons. For D-wave bottom mesons B_2, B_2', and B_3^* we use the average values of Refs. [60] and [58]. Predictions of Refs. [58] and [61] are averaged to obtain the mass of the D-wave bottom–strange mesons B_{s2}, B_{s2}', and B_{s3}^*. The mass values we used can been found here:

$$\begin{aligned} M_B &= 5.280\ \text{GeV}, & M_{B_s} &= 5.367\ \text{GeV}, & M_{B_c} &= 6.276\ \text{GeV},\\ M_{D_2} &= 2.750\ \text{GeV}, & M_{D_2'} &= 2.780\ \text{GeV}, & M_{D_3^*} &= 2.800\ \text{GeV},\\ M_{D_{s2}} &= 2.846\ \text{GeV}, & M_{D_{s2}'} &= 2.872\ \text{GeV}, & M_{D_{s3}^*} &= 2.860\ \text{GeV},\\ M_{B_2} &= 6.060\ \text{GeV}, & M_{B_2'} &= 6.100\ \text{GeV}, & M_{B_3^*} &= 6.050\ \text{GeV},\\ M_{B_{s2}} &= 6.150\ \text{GeV}, & M_{B_{s2}'} &= 6.210\ \text{GeV}, & M_{B_{s3}^*} &= 6.190\ \text{GeV}.\end{aligned}$$

The lifetimes of the initial mesons we used are [59]

$$\begin{aligned}&\tau_{\bar{B}} = 1.519 \times 10^{-12}\ \text{s}, \quad \tau_{\bar{B}_s} = 1.512 \times 10^{-12}\ \text{s},\\ &\tau_{B_c} = 0.452 \times 10^{-12}\ \text{s}.\end{aligned}$$

The involved CKM matrix element values are [59]

$$\begin{aligned}&|V_{ud}| = 0.974,\ |V_{us}| = 0.225,\ |V_{ub}| = 0.0042,\\ &|V_{cd}| = 0.23,\ |V_{cs}| = 1.006,\ |V_{cb}| = 0.041.\end{aligned}$$

In the calculation of non-leptonic decays, the decay constants we used are [47,59]

$$\begin{aligned}&f_\pi = 130.4\ \text{MeV},\ f_K = 156.2\ \text{MeV},\\ &f_\rho = 210\ \text{MeV},\ f_{K^*} = 217\ \text{MeV}.\end{aligned}$$

For the theoretical uncertainties, here we will just discuss the dependence of the final results on our model parameters λ, $\Lambda_{\rm QCD}$ in the Cornell potential, and the constituent quark mass m_b, m_c, m_s, m_d and m_u. The theoretical errors, induced by these model parameters, are determined by varying every parameter by $\pm 5\%$, and then scanning the parameters space to find the maximum deviation. Generally, this theoretical uncertainties can amount to 10–30% for the semi-leptonic decays. The theoretical uncertainties show the robustness of the numerical algorithm.

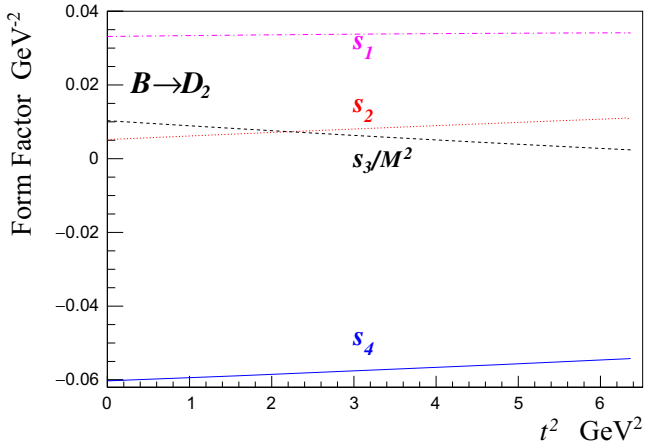

(a) Form Factors for $\bar{B}\to D_2(2^-)$.

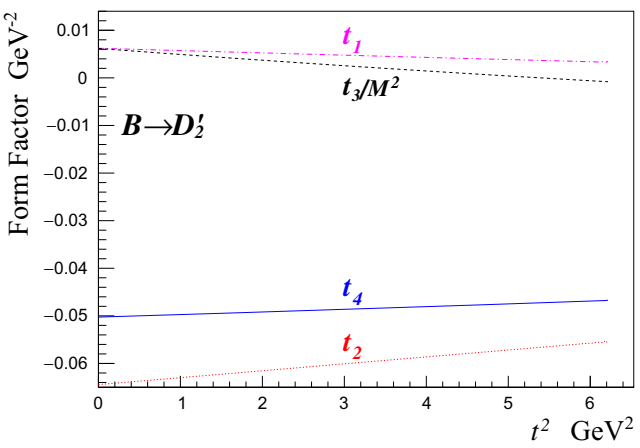

(b) Form Factors for $\bar{B}\to D_2'(2^-)$.

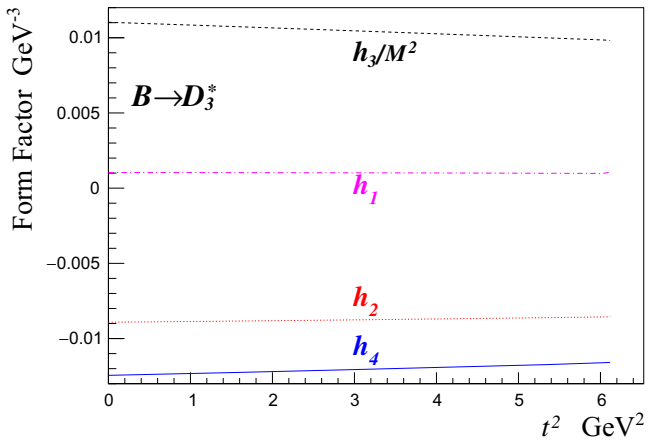

(c) Form Factors for $\bar{B}\to D_3^*(3^-)$.

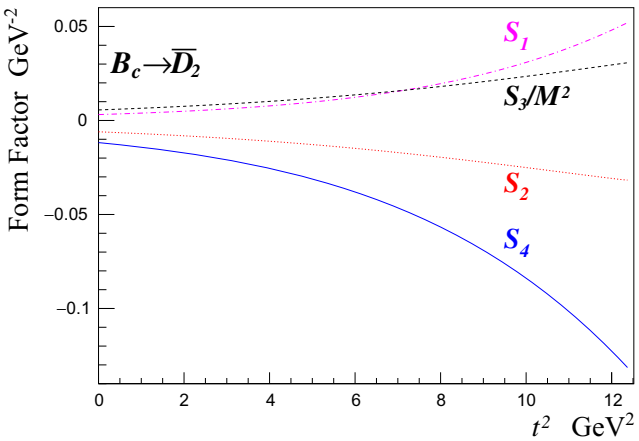

(d) Form Factors for $B_c^-\to\bar{D}_2(2^-)$.

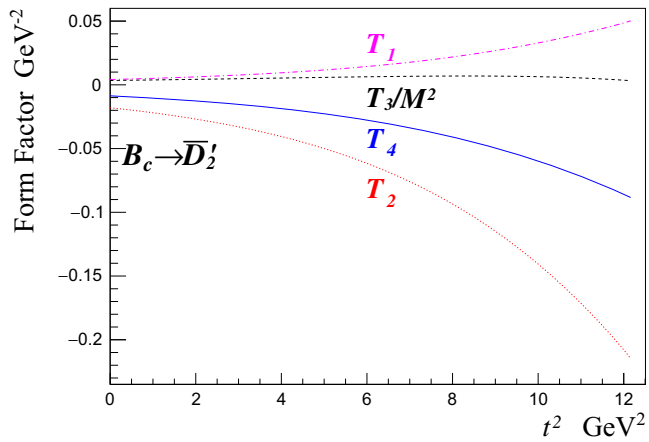

(e) Form Factors for $B_c^-\to\bar{D}_2'(2^-)$.

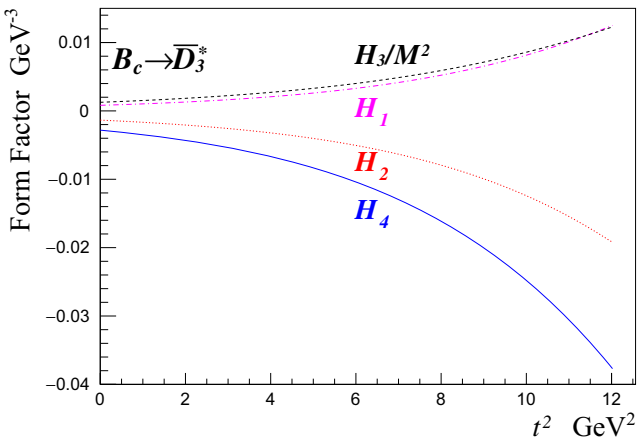

(f) Form Factors for $B_c^-\to\bar{D}_3^*(3^-)$.

Fig. 3 Form factors for transitions $\bar{B}\to D_J^{(*)}\ (2^-,3^-)$ and $B_c^-\to\bar{D}_J^{(*)}\ (2^-,3^-)$. $t^2=(P-P_F)^2$ denotes the square of momentum transfer. To make the dimension consistent, s_3, t_3 and h_3 are divided by $M_{\bar{B}}^2$, S_3, T_3 and H_3 are divided by $M_{B_c}^2$

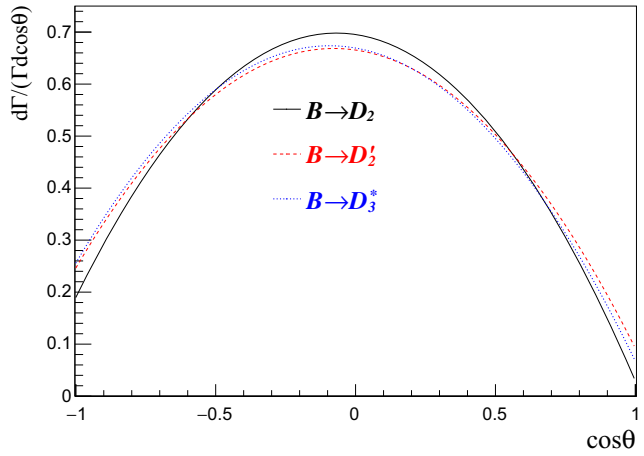

(a) Angular spectrum for $\bar{B}\to D_J^{(*)}e\bar{\nu}$.

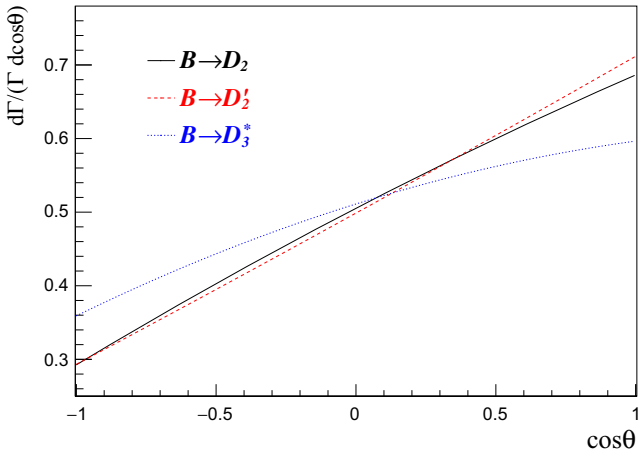

(b) Angular spectrum for $\bar{B}\to D_J^{(*)}\tau\bar{\nu}$.

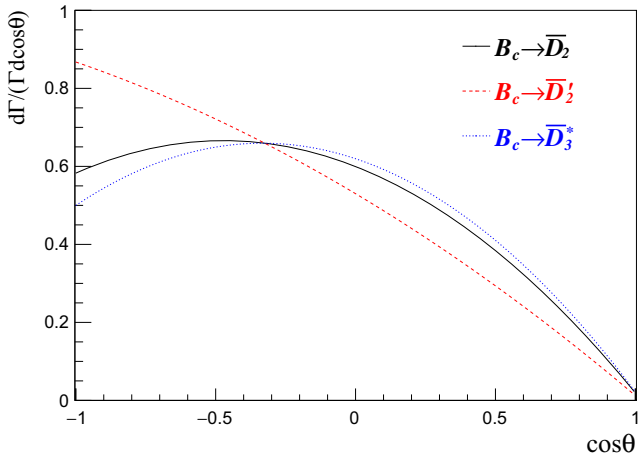

(c) Angular spectrum for $B_c^-\to\bar{D}_J^{(*)}e\nu$ mode.

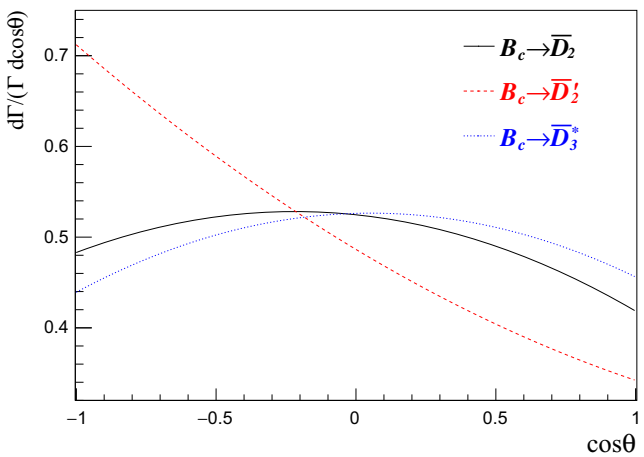

(d) Angular spectrum for $B_c^-\to\bar{D}_J^{(*)}\tau\nu$ mode.

Fig. 4 The spectra of the relative width vs. $\cos\theta$ for semi-leptonic decays $\bar{B}\to D_J^{(*)}$ and $B_c^-\to\bar{D}_J^{(*)}$. θ is the angle between charged lepton ℓ and final charmed meson in the rest frame of $\ell\bar{\nu}$ pair

4.1 Lepton spectra and $A_{\rm FB}$

The distribution of $\bar{B}$ and B_c^- decay width Γ varying along with $\cos\theta$ for the e and τ modes can be seen in Fig. 4, from which we can see that, for the $\bar{B}$ decays, the distribution of the semi-electronic decay widths are much more symmetric than that for the semi-taunic mode. These asymmetries over $\cos\theta$ can also be reflected by the forward–backward asymmetries $A_{\rm FB}$, which are showed in Table 1. We can see that $A_{\rm FB}$ is sensitive to the lepton mass m_ℓ and is a monotonic function of m_ℓ. Considering the absolute values of $A_{\rm FB}$, we find that, for $\bar{B}\to D_J^{(*)}$ and $B_c^-\to\bar{D}_J^{(*)}$, the μ decay mode has the smallest $|A_{\rm FB}|$.

The spectra of decay widths for $\bar{B}$ and B_c^- varying along with $|\boldsymbol{p}_\ell|$, the absolute value of the three-momentum for charged leptons, are showed in Fig. 5. This distribution is almost the same for the $\bar{B}$ decays into D_2, D_2' or D_3^*. For $B_c^-\to\bar{D}_J^{(*)}$, the momentum spectrum of $\bar{D}_2'$ is sharper than that of $\bar{D}_2$ and $\bar{D}_3^*$.

4.2 Branching ratios of semi-leptonic decays

The semi-electronic decay widths we got are $\Gamma(\bar{B}\to D_2e\bar{\nu}_e)=4.9\times10^{-16}$ GeV, $\Gamma(\bar{B}\to D_2'e\bar{\nu}_e)=1.8\times10^{-16}$ GeV, and $\Gamma(\bar{B}\to D_3^*e\bar{\nu}_e)=4.5\times10^{-16}$ GeV. The branching ratios of $\bar{B}$ to D-wave charmed mesons are listed in Table 2. We have listed other results for comparison if available. Our results are about 5 times greater than that in Ref. [22]. It is noticeable that our results for decays into D_2 and D_2' are in the same order, while in the results of QCD sum rules [22] $\mathcal{B}(\bar{B}\to D_2)$ is about 25 times larger than $\mathcal{B}(\bar{B}\to D_2')$. The branching ratios for semi-leptonic decays of $\bar{B}_s$ into D_{s2}, D_{s2}' and D_{s3}^* are listed in Table 3. Our results

Table 1 $A_{\rm FB}$ for semi-leptonic decays of $\bar{B}$, $\bar{B}_s$ and B_c to D-wave heavy–light mesons

Channels	$A_{\rm FB}$	Channels	$A_{\rm FB}$	Channels	$A_{\rm FB}$
$\bar{B}\to\bar{D}_2 e\bar{\nu}$	−0.08	$\bar{B}\to\bar{D}'_2 e\bar{\nu}$	−0.08	$\bar{B}\to\bar{D}^*_3 e\bar{\nu}$	−0.10
$\bar{B}\to\bar{D}_2\mu\bar{\nu}$	−0.05	$\bar{B}\to\bar{D}'_2\mu\bar{\nu}$	−0.05	$\bar{B}\to\bar{D}^*_3\mu\bar{\nu}$	−0.07
$\bar{B}\to\bar{D}_2\tau\bar{\nu}$	0.20	$\bar{B}\to\bar{D}'_2\tau\bar{\nu}$	0.21	$\bar{B}\to\bar{D}^*_3\tau\bar{\nu}$	0.12
$\bar{B}_s\to D_{s2}e\bar{\nu}$	−0.10	$\bar{B}_s\to D'_{s2}e\bar{\nu}$	−0.09	$\bar{B}_s\to D^*_{s3}e\bar{\nu}$	−0.10
$\bar{B}_s\to D_{s2}\mu\bar{\nu}$	−0.07	$\bar{B}_s\to D'_{s2}\mu\bar{\nu}$	−0.06	$\bar{B}_s\to D^*_{s3}\mu\bar{\nu}$	−0.08
$\bar{B}_s\to D_{s2}\tau\bar{\nu}$	0.17	$\bar{B}_s\to D'_{s2}\tau\bar{\nu}$	0.20	$\bar{B}_s\to D^*_{s3}\tau\bar{\nu}$	0.11
$B_c^-\to\bar{D}_2 e\bar{\nu}$	−0.28	$B_c^-\to\bar{D}'_2 e\bar{\nu}$	−0.43	$B_c^-\to\bar{D}^*_3 e\bar{\nu}$	−0.24
$B_c^-\to\bar{D}_2\mu\bar{\nu}$	−0.28	$B_c^-\to\bar{D}'_2\mu\bar{\nu}$	−0.42	$B_c^-\to\bar{D}^*_3\mu\bar{\nu}$	−0.23
$B_c^-\to\bar{D}_2\tau\bar{\nu}$	−0.03	$B_c^-\to\bar{D}'_2\tau\bar{\nu}$	−0.19	$B_c^-\to\bar{D}^*_3\tau\bar{\nu}$	−0.01
$B_c^+\to B_2 e^+\nu$	0.04	$B_c^+\to B'_2 e^+\nu$	−0.07	$B_c^+\to B^*_3 e^+\nu$	0.03
$B_c^+\to B_2\mu^+\nu$	0.23	$B_c^+\to B'_2\mu^+\nu$	0.18	$B_c^+\to B^*_3\mu^+\nu$	0.24
$B_c^+\to B_{s2}e^+\nu$	0.03	$B_c^+\to B'_{s2}e^+\nu$	−0.03	$B_c^+\to B^*_{s3}e^+\nu$	0.01

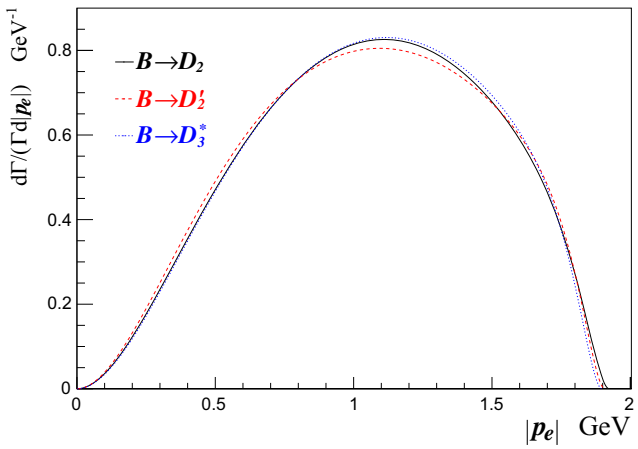

(a) Momentum spectrum for decay $\bar{B}\to D_J^{(*)}e\bar{\nu}$.

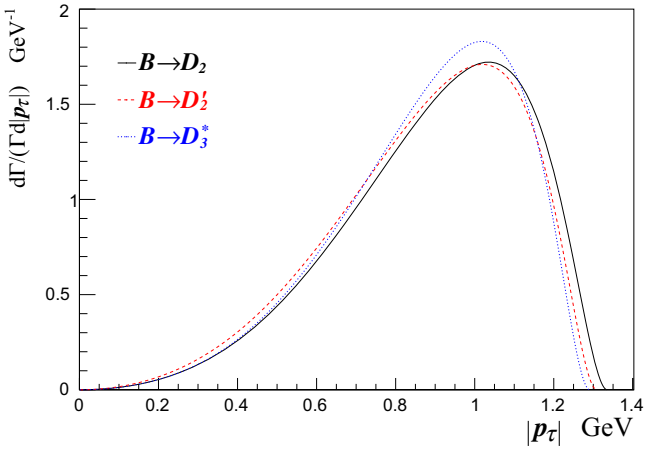

(b) Momentum spectrum for decay $\bar{B}\to D_J^{(*)}\tau\bar{\nu}$.

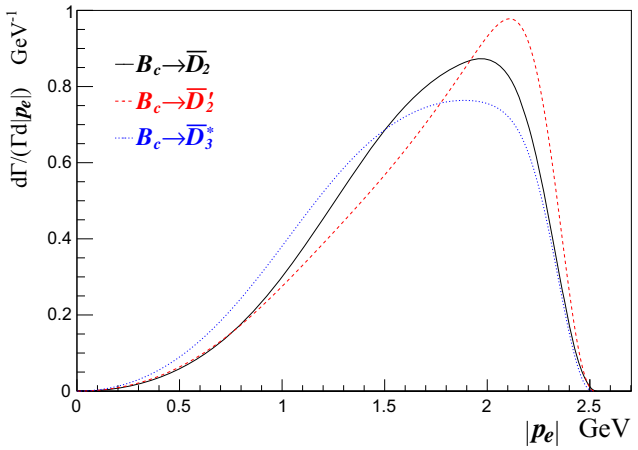

(c) Momentum spectrum for decay $B_c^-\to\bar{D}_J^{(*)}e\bar{\nu}$.

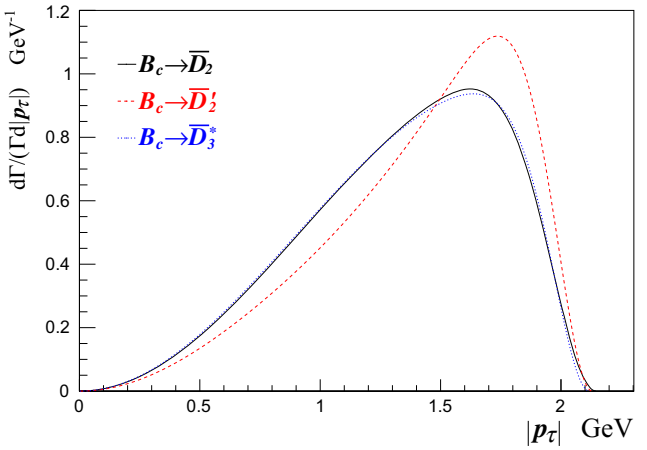

(d) Momentum spectrum for decay $B_c^-\to\bar{D}_J^{(*)}\tau\bar{\nu}$.

Fig. 5 The spectra of the relative width vs. $|\boldsymbol{p}_\ell|$, the absolute value of charged lepton's 3-momentum, in transitions $\bar{B}\to D_J^{(*)}$ and $B_c^-\to\bar{D}_J^{(*)}$

Table 2 Branching ratios of $\bar{B}$ semi-leptonic decays with $\tau_{\bar{B}} = 1.519 \times 10^{-12}$ s

Channels	Ours	Ref. [22]	Ref. [21]	Ref. [24]	Ref. [25]
$\bar{B} \to D_2 e\bar{\nu}$	$1.1^{-0.3}_{+0.3} \times 10^{-3}$	1.5×10^{-4}	1×10^{-5}	–	–
$\bar{B} \to D_2 \mu\bar{\nu}$	$1.1^{-0.3}_{+0.3} \times 10^{-3}$	1.5×10^{-5}	1×10^{-5}	–	–
$\bar{B} \to D_2 \tau\bar{\nu}$	$8.0^{-2.0}_{+2.0} \times 10^{-6}$	–	–	–	–
$\bar{B} \to D'_2 e\bar{\nu}$	$4.1^{-0.8}_{+0.9} \times 10^{-4}$	6×10^{-6}	–	2×10^{-6}	6×10^{-5}
$\bar{B} \to D'_2 \mu\bar{\nu}$	$4.1^{-0.8}_{+0.9} \times 10^{-4}$	6×10^{-6}	–	2×10^{-6}	–
$\bar{B} \to D'_2 \tau\bar{\nu}$	$2.7^{-0.4}_{+0.5} \times 10^{-6}$	–	–	–	–
$\bar{B} \to D^*_3 e\bar{\nu}$	$1.0^{-0.2}_{+0.2} \times 10^{-3}$	2.1×10^{-4}	1×10^{-5}	–	–
$\bar{B} \to D^*_3 \mu\bar{\nu}$	$1.0^{-0.2}_{+0.2} \times 10^{-3}$	2.1×10^{-4}	1×10^{-5}	–	–
$\bar{B} \to D^*_3 \tau\bar{\nu}$	$5.4^{-0.9}_{+1.0} \times 10^{-6}$	–	–	–	–

Table 3 Branching ratios of $\bar{B}_s$ semi-leptonic decays with $\tau_{\bar{B}_s} = 1.512 \times 10^{-12}$ s

Channels	Ours	Ref. [23]
$\bar{B}_s \to D_{s2} e\bar{\nu}$	$1.7^{-0.5}_{+0.5} \times 10^{-3}$	1.02×10^{-4}
$\bar{B}_s \to D_{s2} \mu\bar{\nu}$	$1.7^{-0.5}_{+0.4} \times 10^{-3}$	1.02×10^{-4}
$\bar{B}_s \to D_{s2} \tau\bar{\nu}$	$1.3^{-0.4}_{+0.4} \times 10^{-5}$	–
$\bar{B}_s \to D'_{s2} e\bar{\nu}$	$5.2^{-1.5}_{+1.6} \times 10^{-4}$	3.4×10^{-7}
$\bar{B}_s \to D'_{s2} \mu\bar{\nu}$	$5.1^{-1.5}_{+1.6} \times 10^{-4}$	3.4×10^{-7}
$\bar{B}_s \to D'_{s2} \tau\bar{\nu}$	$3.4^{-1.0}_{+1.1} \times 10^{-6}$	–
$\bar{B}_s \to D^*_{s3} e\bar{\nu}$	$1.5^{-0.4}_{+0.4} \times 10^{-3}$	3.46×10^{-4}
$\bar{B}_s \to D^*_{s3} \mu\bar{\nu}$	$1.4^{-0.4}_{+0.4} \times 10^{-3}$	3.46×10^{-4}
$\bar{B}_s \to D^*_{s3} \tau\bar{\nu}$	$9.4^{-2.5}_{+2.8} \times 10^{-6}$	–

for $\bar{B}_s$ to D-wave charm–strange mesons are also much larger than the results of QCD sum rules in Ref. [23].

The branching ratios for B_c to D-wave $\bar{D}_J^{(*)}$ are listed in Table 4. The branching ratios for semi-leptonic decays of B_c^- to $\bar{D}_2$ and $\bar{D}_3^*$ are in the order of 10^{-5}, and for $B_c^- \to D'_2$ the results are in the order of 10^{-6}. These results are about 100 times smaller than those for the $\bar{B}_{(s)}$ decays owing to the different CKM matrix elements.

For completeness of this research, we also give the corresponding results for B_c to the D-wave $B_J^{(*)}$ and $B_{sJ}^{(*)}$ in Table 4, although their branching ratios are quite small due to the tiny phase space. For D-wave bottom mesons, the semi-taunic mode is not available and for the D-wave bottom–strange mesons, both the μ and the τ modes are unavailable since the constraints of phase space. The branching ratios for $B_c^+ \to B_J^{(*)}$ are less than 10^{-8} and those for $B_c^+ \to B_{sJ}^{(*)}$ are less than 10^{-9}. Based on our results, the possibilities for the D-wave bottomed mesons to be detected in B_c decays are quite small by current experiments.

The ratio $\mathscr{R}[D_J^{(*)}]$, defined as the ratio of semi-taunic branching fraction over semi-electronic branching fraction for decay $\bar{B} \to D_J^{(*)}$, namely, $\mathscr{R}[D_J^{(*)}] = \frac{\mathcal{B}[\bar{B} \to D_J^{(*)} \tau^- \bar{\nu}_\tau]}{\mathcal{B}[\bar{B} \to D_J^{(*)} e^- \bar{\nu}_e]}$, may hint the new physics [26,27]. We present these ratios for decays to D-wave charmed mesons in Table 5, from which we can see that $\mathscr{R}[D_J^{(*)}]$ for $\bar{B}$ decays and $\mathscr{R}[D_{sJ}^{(*)}]$ for $\bar{B}_s$ decays are almost the same and in the order of 10^{-3}, while $\mathscr{R}[\bar{D}_J^{(*)}]$ for B_c^- decays are in the order of 10^{-1}. This big difference is mainly due to the phase space. By simple integral over the phase space, we can find that, the phase space ratio of semi-taunic decay over semi-electronic decay for the B_c^- meson is about 30 times larger than that for the $\bar{B}$ or $\bar{B}_s$ meson.

Table 4 Semi-leptonic decay branching ratios of B_c to D-wave heavy–light mesons with $\tau_{B_c} = 0.452 \times 10^{-12}$ s

Channels	Br	Channels	Br	Channels	Br
$B_c^- \to \bar{D}_2 e\bar{\nu}$	$2.2^{-0.4}_{+0.7} \times 10^{-5}$	$B_c^- \to \bar{D}'_2 e\bar{\nu}$	$4.0^{-0.9}_{+1.6} \times 10^{-6}$	$B_c^- \to \bar{D}^*_3 e\bar{\nu}$	$1.2^{-0.2}_{+0.4} \times 10^{-5}$
$B_c^- \to \bar{D}_2 \mu\bar{\nu}$	$2.2^{-0.4}_{+0.7} \times 10^{-5}$	$B_c^- \to \bar{D}'_2 \mu\bar{\nu}$	$4.0^{-0.9}_{+1.6} \times 10^{-6}$	$B_c^- \to \bar{D}^*_3 \mu\bar{\nu}$	$1.2^{-0.2}_{+0.4} \times 10^{-5}$
$B_c^- \to \bar{D}_2 \tau\bar{\nu}$	$7.7^{-1.5}_{+2.6} \times 10^{-6}$	$B_c^- \to \bar{D}'_2 \tau\bar{\nu}$	$1.2^{-0.3}_{+0.5} \times 10^{-6}$	$B_c^- \to \bar{D}^*_3 \tau\bar{\nu}$	$3.1^{-0.7}_{+1.1} \times 10^{-6}$
$B_c^+ \to B_2 e^+\nu$	$9.4^{-1.0}_{+0.7} \times 10^{-9}$	$B_c^+ \to B'_2 e^+\nu$	$1.3^{-0.3}_{+0.3} \times 10^{-10}$	$B_c^+ \to B^*_3 e^+\nu$	$1.4^{-0.3}_{+0.3} \times 10^{-10}$
$B_c^+ \to B_2 \mu^+\nu$	$1.7^{-0.2}_{+0.1} \times 10^{-9}$	$B_c^+ \to B'_2 \mu^+\nu$	$7.6^{-0.7}_{+0.7} \times 10^{-12}$	$B_c^+ \to B^*_3 \mu^+\nu$	$2.0^{-0.4}_{+0.4} \times 10^{-11}$
$B_c^+ \to B_{s2} e^+\nu$	$3.3^{-0.2}_{+0.2} \times 10^{-9}$	$B_c^+ \to B'_{s2} e^+\nu$	$3.2^{-0.4}_{+0.4} \times 10^{-12}$	$B_c^+ \to B^*_{s3} e^+\nu$	$5.6^{-1.7}_{+1.7} \times 10^{-13}$

Table 5 $\mathscr{R}[D_J^{(*)}] = \frac{\mathscr{B}[\bar{B}\to D_J^{(*)}\tau\bar{\nu}_\tau]}{\mathscr{B}[\bar{B}\to D_J^{(*)}e\bar{\nu}_e]}$, $\mathscr{R}[D_{sJ}^{(*)}] = \frac{\mathscr{B}[\bar{B}_s\to D_{sJ}^{(*)}\tau\bar{\nu}_\tau]}{\mathscr{B}[\bar{B}_s\to D_{sJ}^{(*)}e\bar{\nu}_e]}$, and $\mathscr{R}[\bar{D}_J^{(*)}] = \frac{\mathscr{B}[B_c^-\to \bar{D}_J^{(*)}\tau\bar{\nu}_\tau]}{\mathscr{B}[B_c^-\to \bar{D}_J^{(*)}e\bar{\nu}_e]}$, ratios of semi-taunic branching ratio to semi-electronic branching ratio for the $\bar{B}$, $\bar{B}_s$, and B_c^- to D-wave charmed mesons

Modes	D_2	D_2'	D_3^*	D_{s2}	D_{s2}'	D_{s3}^*	$\bar{D}_2$	$\bar{D}_2'$	$\bar{D}_3^*$
$\mathscr{R}$	0.0071	0.0065	0.0052	0.0079	0.0066	0.0064	0.35	0.29	0.25

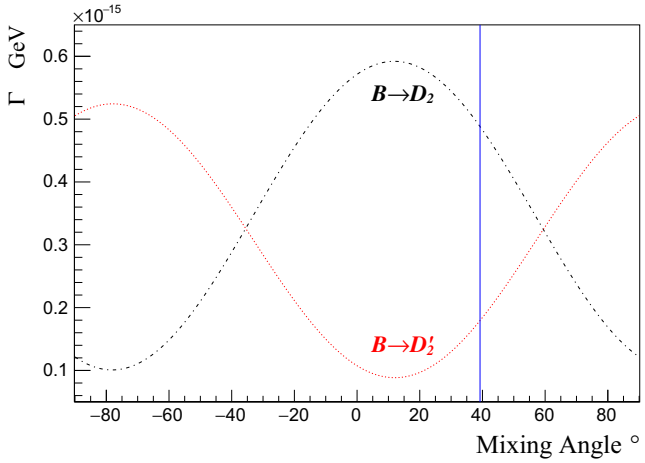

(a) $\bar{B}\to D_2^{(\prime)}e\bar{\nu}$ decay width vs mixing angle.

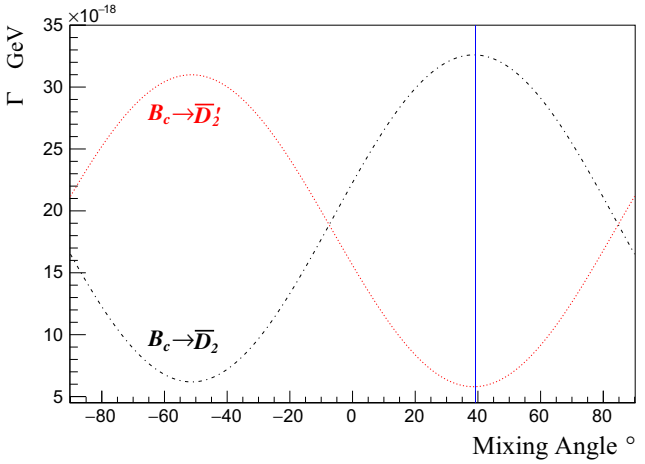

(b) $B_c^-\to\bar{D}_2^{(\prime)}e\bar{\nu}$ decay width vs mixing angle.

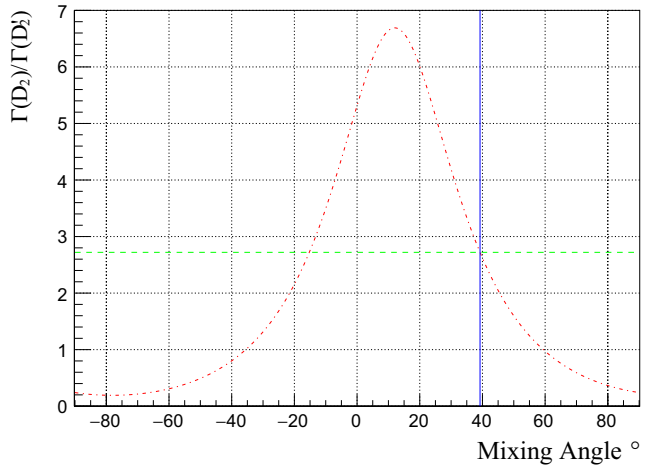

(c) $\Gamma(\bar{B}\to D_2e\bar{\nu})/\Gamma(\bar{B}\to D_2'e\bar{\nu})$ vs mixing angle.

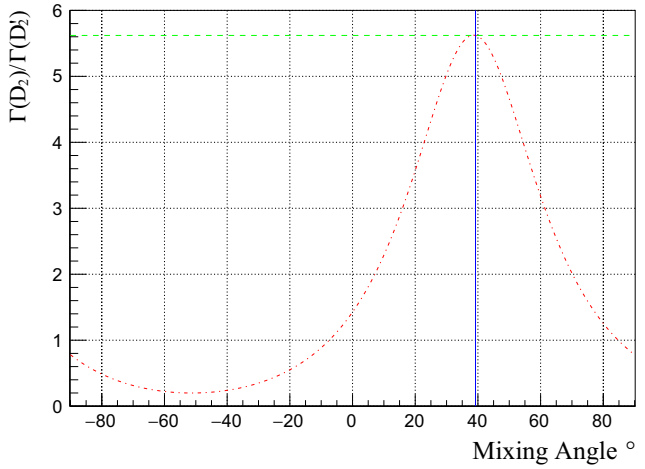

(d) $\Gamma(B_c^-\to\bar{D}_2e\bar{\nu})/\Gamma(B_c^-\to\bar{D}_2'e\bar{\nu})$ vs mixing angle.

Fig. 6 Decay widths $\Gamma[\bar{B}\to D_2(D_2')e\bar{\nu}]$ and $\Gamma[B_c^-\to\bar{D}_2(\bar{D}_2')e\bar{\nu}]$ vary along with the mixing angle. The *vertical solid line* shows the results when mixing angle $\alpha = 39.23°$, where the decay width ratio is 2.73 for $\bar{B}\to D_2(D_2')e\bar{\nu}$ and 5.63 for $B_c^-\to\bar{D}_2(\bar{D}_2')e\bar{\nu}$

The decay widths for the $\bar{B}_{(s)}$ or B_c to 2^- states mesons are dependent on the mixing angle α, which can be showed by Fig. 6a, b. This dependence for the $\bar{B}$ decays can be described by the following equations:

$$\Gamma(\bar{B}\to D_2e\bar{\nu}) = \Gamma_1\big[1+\lambda_1\cos(2\alpha+\Theta_1)\big], \quad (29)$$

$$\Gamma(\bar{B}\to D_2'e\bar{\nu}) = \Gamma_2\big[1-\lambda_2\cos(2\alpha+\Theta_2)\big]. \quad (30)$$

Our fit results show that the parameters are

$$\Gamma_1 = 3.46\times10^{-16},\quad \lambda_1 = 0.709,\quad \Theta_1 = -23.7°,$$
$$\Gamma_2 = 3.06\times10^{-16},\quad \lambda_2 = 0.711,\quad \Theta_2 = -24.1°.$$

The tiny differences in parameters for D_2 and D_2' come from the small difference between m_{D_2} and $m_{D_2'}$. In Fig. 6c, d, we also show the ratios $\frac{\Gamma(\bar{B}\to D_2e\bar{\nu})}{\Gamma(\bar{B}\to D_2'e\bar{\nu})}$ and $\frac{\Gamma(B_c^-\to\bar{D}_2e\bar{\nu})}{\Gamma(B_c^-\to\bar{D}_2'e\bar{\nu})}$, which are very sensitive to the mixing angle.

Table 6 Non-leptonic decay widths of $\bar{B}$, $\bar{B}_s$ and B_c to D-wave heavy–light meson with general Wilson coefficient a_1

Channels	Width	Channels	Width	Channels	$\times a_1^2$ [GeV] Width
$\bar{B}\to D_2\pi^-$	$2.8^{-0.7}_{+0.7}\times10^{-16}$	$\bar{B}\to D_2'\pi^-$	$9.8^{-2.0}_{+2.2}\times10^{-17}$	$\bar{B}\to D_3^*\pi^-$	$2.2^{-0.4}_{+0.4}\times10^{-16}$
$\bar{B}\to D_2K^-$	$2.0^{-0.5}_{+0.5}\times10^{-17}$	$\bar{B}\to D_2'K^-$	$6.7^{-1.4}_{+1.5}\times10^{-18}$	$\bar{B}\to D_3^*K^-$	$1.4^{-0.3}_{+0.3}\times10^{-17}$
$\bar{B}\to D_2\rho^-$	$5.5^{-1.4}_{+1.4}\times10^{-16}$	$\bar{B}\to D_2'\rho^-$	$2.0^{-0.4}_{+0.4}\times10^{-16}$	$\bar{B}\to D_3^*\rho^-$	$4.7^{-0.8}_{+0.9}\times10^{-16}$
$\bar{B}\to D_2K^{*-}$	$2.9^{-0.7}_{+0.7}\times10^{-17}$	$\bar{B}\to D_2'K^{*-}$	$1.0^{-0.2}_{+0.2}\times10^{-17}$	$\bar{B}\to D_3^*K^{*-}$	$2.5^{-0.4}_{+0.5}\times10^{-17}$
$\bar{B}_s\to D_{s2}\pi^-$	$4.0^{-1.0}_{+1.1}\times10^{-16}$	$\bar{B}_s\to D_{s2}'\pi^-$	$1.2^{-0.4}_{+0.4}\times10^{-16}$	$\bar{B}_s\to D_{s3}^*\pi^-$	$2.9^{-0.8}_{+0.7}\times10^{-16}$
$\bar{B}_s\to D_{s2}K^-$	$2.8^{-0.8}_{+0.7}\times10^{-17}$	$\bar{B}_s\to D_{s2}'K^-$	$8.2^{-2.4}_{+2.5}\times10^{-18}$	$\bar{B}_s\to D_{s3}^*K^-$	$1.9^{-0.5}_{+0.5}\times10^{-17}$
$\bar{B}_s\to D_{s2}\rho^-$	$8.1^{-2.3}_{+2.1}\times10^{-16}$	$\bar{B}_s\to D_{s2}'\rho^-$	$2.4^{-0.7}_{+0.8}\times10^{-16}$	$\bar{B}_s\to D_{s3}^*\rho^-$	$6.4^{-1.7}_{+1.7}\times10^{-16}$
$\bar{B}_s\to D_{s2}K^{*-}$	$4.2^{-1.2}_{+1.1}\times10^{-17}$	$\bar{B}_s\to D_{s2}'K^{*-}$	$1.3^{-0.4}_{+0.4}\times10^{-17}$	$\bar{B}_s\to D_{s3}^*K^{*-}$	$3.4^{-0.9}_{+0.9}\times10^{-17}$
$B_c^-\to\bar{D}_2\pi^-$	$1.1^{-0.4}_{+0.7}\times10^{-18}$	$B_c^-\to\bar{D}_2'\pi^-$	$2.5^{-0.7}_{+1.3}\times10^{-19}$	$B_c^-\to\bar{D}_3^*\pi^-$	$1.1^{-0.3}_{+0.5}\times10^{-18}$
$B_c^-\to\bar{D}_2K^-$	$9.0^{-0.3}_{+0.5}\times10^{-20}$	$B_c^-\to\bar{D}_2'K^-$	$2.0^{-0.6}_{+1.0}\times10^{-20}$	$B_c^-\to\bar{D}_3^*K^-$	$8.4^{-2.2}_{+4.0}\times10^{-20}$
$B_c^-\to\bar{D}_2\rho^-$	$3.5^{-1.1}_{+1.9}\times10^{-18}$	$B_c^-\to\bar{D}_2'\rho^-$	$7.8^{-2.2}_{+3.9}\times10^{-19}$	$B_c^-\to\bar{D}_3^*\rho^-$	$3.1^{-0.8}_{+1.4}\times10^{-18}$
$B_c^-\to\bar{D}_2K^{*-}$	$2.1^{-0.6}_{+1.1}\times10^{-19}$	$B_c^-\to\bar{D}_2'K^{*-}$	$4.7^{-1.3}_{+2.3}\times10^{-20}$	$B_c^-\to\bar{D}_3^*K^{*-}$	$1.9^{-0.5}_{+0.8}\times10^{-19}$
$B_c^+\to B_2\pi^+$	$1.4^{-0.1}_{+0.1}\times10^{-19}$	$B_c^+\to B_2'\pi^+$	$1.3^{-0.3}_{+0.2}\times10^{-21}$	$B_c^+\to B_3^*\pi^+$	$1.9^{-0.4}_{+0.4}\times10^{-21}$

Table 7 Branching ratios of non-leptonic decays for $\bar{B}$, $\bar{B}_s$ and B_c to D-wave heavy–light mesons. $a_1^b=1.14$ for b quark decay and $a_1^c=1.2$ for c quark decay

Channels	Br	Channels	Br	Channels	Br
$\bar{B}\to D_2\pi^-$	$8.5^{-2.2}_{+2.1}\times10^{-4}$	$\bar{B}\to D_2'\pi^-$	$2.9^{-0.6}_{+0.6}\times10^{-4}$	$\bar{B}\to D_3^*\pi^-$	$6.5^{-1.2}_{+1.2}\times10^{-4}$
$\bar{B}\to D_2K^-$	$5.9^{-1.5}_{+1.4}\times10^{-5}$	$\bar{B}\to D_2'K^-$	$2.0^{-0.4}_{+0.4}\times10^{-5}$	$\bar{B}\to D_3^*K^-$	$4.3^{-0.8}_{+0.8}\times10^{-5}$
$\bar{B}\to D_2\rho^-$	$1.7^{-0.4}_{+0.4}\times10^{-3}$	$\bar{B}\to D_2'\rho^-$	$5.9^{-1.2}_{+1.3}\times10^{-4}$	$\bar{B}\to D_3^*\rho^-$	$1.4^{-0.3}_{+0.3}\times10^{-3}$
$\bar{B}\to D_2K^{*-}$	$8.6^{-2.2}_{+2.1}\times10^{-5}$	$\bar{B}\to D_2'K^{*-}$	$3.1^{-0.6}_{+0.7}\times10^{-5}$	$\bar{B}\to D_3^*K^{*-}$	$7.5^{-1.3}_{+1.4}\times10^{-5}$
$\bar{B}_s\to D_{s2}\pi^-$	$1.2^{-0.3}_{+0.3}\times10^{-3}$	$\bar{B}_s\to D_{s2}'\pi^-$	$3.6^{-1.0}_{+1.1}\times10^{-4}$	$\bar{B}_s\to D_{s3}^*\pi^-$	$8.5^{-2.3}_{+2.2}\times10^{-4}$
$\bar{B}_s\to D_{s2}K^-$	$8.3^{-2.3}_{+2.1}\times10^{-5}$	$\bar{B}_s\to D_{s2}'K^-$	$2.5^{-0.7}_{+0.7}\times10^{-5}$	$\bar{B}_s\to D_{s3}^*K^-$	$5.7^{-1.6}_{+1.5}\times10^{-5}$
$\bar{B}_s\to D_{s2}\rho^-$	$2.4^{-0.7}_{+0.6}\times10^{-3}$	$\bar{B}_s\to D_{s2}'\rho^-$	$7.3^{-2.1}_{+2.2}\times10^{-4}$	$\bar{B}_s\to D_{s3}^*\rho^-$	$1.9^{-0.5}_{+0.5}\times10^{-3}$
$\bar{B}_s\to D_{s2}K^{*-}$	$1.3^{-0.4}_{+0.3}\times10^{-4}$	$\bar{B}_s\to D_{s2}'K^{*-}$	$3.8^{-1.1}_{+1.2}\times10^{-5}$	$\bar{B}_s\to D_{s3}^*K^{*-}$	$1.0^{-0.3}_{+0.3}\times10^{-4}$
$B_c^-\to\bar{D}_2\pi^-$	$1.0^{-0.3}_{+0.6}\times10^{-6}$	$B_c^-\to\bar{D}_2'\pi^-$	$2.2^{-0.6}_{+1.2}\times10^{-7}$	$B_c^-\to\bar{D}_3^*\pi^-$	$9.6^{-2.6}_{+4.6}\times10^{-7}$
$B_c^-\to\bar{D}_2K^-$	$8.0^{-2.5}_{+4.6}\times10^{-8}$	$B_c^-\to\bar{D}_2'K^-$	$1.7^{-0.5}_{+0.9}\times10^{-8}$	$B_c^-\to\bar{D}_3^*K^-$	$7.5^{-0.2}_{+3.5}\times10^{-8}$
$B_c^-\to\bar{D}_2\rho^-$	$3.1^{-1.0}_{+1.7}\times10^{-6}$	$B_c^-\to\bar{D}_2'\rho^-$	$6.9^{-2.0}_{+3.5}\times10^{-7}$	$B_c^-\to\bar{D}_3^*\rho^-$	$2.8^{-0.7}_{+1.3}\times10^{-6}$
$B_c^-\to\bar{D}_2K^{*-}$	$1.9^{-0.6}_{+1.0}\times10^{-7}$	$B_c^-\to\bar{D}_2'K^{*-}$	$4.2^{-1.2}_{+2.0}\times10^{-8}$	$B_c^-\to\bar{D}_3^*K^{*-}$	$1.7^{-0.4}_{+0.7}\times10^{-7}$
$B_c^+\to B_2\pi^+$	$1.4^{-0.1}_{+0.1}\times10^{-7}$	$B_c^+\to B_2'\pi^+$	$1.3^{-0.2}_{+0.2}\times10^{-9}$	$B_c^+\to B_3^*\pi^+$	$1.9^{-0.4}_{+0.4}\times10^{-9}$

4.3 Non-leptonic decay widths and branching ratios

The non-leptonic decay widths are listed in Table 6, where we have kept the Wilson coefficient a_1 in order to facilitate comparison with other models. The corresponding branching ratios are listed in Table 7, where we have specified the values $a_1^b=1.14$ for the $b\to c(u)$ transition and $a_1^c=1.2$ for the $c\to d(s)$ transition [47]. From the non-leptonic decay results we can see that, with the same final D meson, the ρ mode has the largest branching ratio and can reach order 10^{-3} in $\bar{B}_{(s)}$ decays, and order 10^{-6} in B_c decay. When the light mesons have the same quark constituents, the width for decay into vector meson (ρ, K^*) mode is about 2–3 times greater than its pseudoscalar meson (π, K) mode.

5 Summary

In this work we calculated semi-leptonic and non-leptonic decays of $\bar{B}_{(s)}$ into D-wave charmed mesons ($D_{(s)2}$, $D'_{(s)2}$, $D^*_{(s)3}$) and B_c into D-wave charmed and bottomed excited mesons. Form factors of the hadronic transition are calculated by instantaneous Bethe–Salpeter methods. The semi-electronic branching ratios for $\bar{B}_{(s)}\to D^{(*)}_{(s)J}$ we got are about

order 10^{-3}, and for B_c to D-wave charmed mesons are about order 10^{-5}. The non-leptonic branching ratios for decays to ρ mode can reach the order of 10^{-3} for $\bar{B}_{(s)}$ decays. So the D-wave D and D_s mesons can hopefully be detected in $\bar{B}_{(s)}$ decays by current experiments. Our results reveal the branching fractions for B_c to D-wave bottomed mesons are less than 10^{-8}, which makes the D-wave bottomed mesons almost impossible to be discovered in B_c decays by current experiments.

We also present the angular distribution and charged lepton spectra for $\bar{B}$ and B_c decays. The 2^- states D_2 and D_2' are the mixing states of $^1D_2 - {}^3D_2$, so we present the dependence of the decay width varying along with the mixing angle. Based on our results, the semi-leptontic and non-leptonic branching ratios for $\bar{B}_{(s)}$ decays to the D-wave charm and charm–strange mesons have reached the experimental detection thresholds. These results would be helpful in future detecting and understanding these new D-wave excited $D_{(s)}$ mesons.

Acknowledgements This work was supported in part by the National Natural Science Foundation of China (NSFC) under Grant Nos. 11405037, 11575048 and 11505039, and in part by PIRS of HIT Nos. T201405, A201409, and B201506.

A Expressions for N_is in the hadronic tensor $H_{\mu\nu}$

The hadronic tensor N_i $(i = 1, 2, 4, 5, 6)$ for $\bar{B}$ to D_2 meson are

$$N_1 = \frac{2M^4 \boldsymbol{p}_F^4 s_1^2}{3M_F^4} - \frac{4M^2 \boldsymbol{p}_F^2 s_1 s_3}{3M_F^2} - \frac{1}{2} M^2 \boldsymbol{p}_F^2 s_4^2 + \frac{s_3^2}{6}, \tag{A.1}$$

$$N_2 = \frac{2E_F M^3 \boldsymbol{p}_F^2 s_1 s_3}{3M_F^4} + \frac{E_F M^3 \boldsymbol{p}_F^2 s_4^2}{2M_F^2} - \frac{E_F M s_3^2}{6M_F^2} + \frac{2M^4 \boldsymbol{p}_F^4 s_1 s_2}{3M_F^4} - \frac{2M^2 \boldsymbol{p}_F^2 s_2 s_3}{3M_F^2}, \tag{A.2}$$

$$N_4 = \frac{4E_F M^3 \boldsymbol{p}_F^2 s_2 s_3}{3M_F^4} + \frac{2M^4 \boldsymbol{p}_F^4 s_2^2}{3M_F^4} - \frac{M^4 \boldsymbol{p}_F^2 s_4^2}{2M_F^2} + \frac{M^2 s_3^2 (M_F^2 + 4\boldsymbol{p}_F^2)}{6M_F^4}, \tag{A.3}$$

$$N_5 = -\frac{M^4 \boldsymbol{p}_F^4 s_4^2}{2M_F^2} - \frac{M^2 \boldsymbol{p}_F^2 s_3^2}{2M_F^2}, \tag{A.4}$$

$$N_6 = -\frac{M^2 \boldsymbol{p}_F^2 s_3 s_4}{M_F^2}. \tag{A.5}$$

Here $\boldsymbol{p}_F$ denotes the three-momentum of the final D systems and $E_F = \sqrt{M_F^2 + \boldsymbol{p}_F^2}$. For $\bar{B}$ to D_2' the relations between N_i and form factors t_k $(k = 1, 2, 3, 4)$ have the same form as that for D_2, just s_k are replaced with t_k. Both s_k and t_k are functions of $q_\perp'^2$.

The hadronic tensor N_i for $\bar{B}$ to D_3^* are expressed with form factors h_k $(k = 1, 2, 3, 4)$ as

$$N_1 = \frac{2M^6 \boldsymbol{p}_F^6 h_1^2}{5M_F^6} - \frac{4M^4 \boldsymbol{p}_F^4 h_1 h_3}{5M_F^4} - \frac{4M^4 \boldsymbol{p}_F^4 h_4^2}{15M_F^2} + \frac{2M^2 \boldsymbol{p}_F^2 h_3^2}{15M_F^2}, \tag{A.6}$$

$$N_2 = \frac{2E_F M^5 \boldsymbol{p}_F^4 h_1 h_3}{5M_F^6} + \frac{4E_F M^5 \boldsymbol{p}_F^4 h_4^2}{15M_F^4} - \frac{2E_F M^3 \boldsymbol{p}_F^2 h_3^2}{15M_F^4} + \frac{2M^6 \boldsymbol{p}_F^6 h_1 h_2}{5M_F^6} - \frac{2M^4 \boldsymbol{p}_F^4 h_2 h_3}{5M_F^4}, \tag{A.7}$$

$$N_4 = \frac{4E_F M^5 \boldsymbol{p}_F^4 h_2 h_3}{5M_F^6} + \frac{2M^6 \boldsymbol{p}_F^6 h_2^2}{5M_F^6} - \frac{4M^6 \boldsymbol{p}_F^4 h_4^2}{15M_F^4} + \frac{2M^4 \boldsymbol{p}_F^2 h_3^2 (M_F^2 + 3\boldsymbol{p}_F^2)}{15M_F^6}, \tag{A.8}$$

$$N_5 = -\frac{4M^6 \boldsymbol{p}_F^6 h_4^2}{15M_F^4} - \frac{4M^4 \boldsymbol{p}_F^4 h_3^2}{15M_F^4}, \tag{A.9}$$

$$N_6 = -\frac{8M^4 \boldsymbol{p}_F^4 h_3 h_4}{15M_F^4}. \tag{A.10}$$

.

B Full Salpeter equations and the numerical solutions

B.1 Salpeter equations

The Salpeter wave function $\varphi(q_\perp)$ is related to the BS wave function $\Psi(q)$ by the following definition:

$$\varphi(q_\perp) = \mathrm{i} \int \frac{\mathrm{d}q_P}{2\pi} \Psi(q), \quad \eta(q_\perp) = \int \frac{\mathrm{d}^3 k_\perp}{(2\pi)^3} \varphi(k_\perp) V(|q_\perp - k_\perp|), \tag{B.1}$$

where the 3-dimensional integration $\eta(q_\perp)$ can be understood as the BS vertex for bound states, and $V(|q_\perp - k_\perp|)$ denotes the instantaneous interaction kernel.

The projection operators $\Lambda_i^\pm(q_\perp)$ ($i = 1$ for quark and 2 for anti-quark) are defined as

$$\Lambda_i^\pm = \frac{1}{2\omega_i} \left[\frac{\not{P}}{M} \omega_i \pm (-1)^{i+1} (m_i + \not{q}_\perp) \right]. \tag{B.2}$$

Then we define the four wave functions $\varphi^{\pm\pm}$ by φ and $\Lambda_i^{\pm}$ as

$$\varphi^{\pm\pm} \equiv \Lambda_1^{\pm}(q_\perp)\frac{\not{P}}{M}\varphi(q_\perp)\frac{\not{P}}{M}\Lambda_2^{\pm}(q_\perp), \tag{B.3}$$

where φ^{++} and φ^{--} are called the positive and negative Salpeter wave functions, respectively. And we can easily check that $\varphi = \varphi^{++} + \varphi^{-+} + \varphi^{+-} + \varphi^{--}$.

The full coupled Salpeter equations then can be expressed as [31]

$$\varphi^{+-} = \varphi^{-+} = 0, \tag{B.4}$$
$$(M - \omega_1 - \omega_2)\varphi^{++} = +\Lambda_1^{+}(q_\perp)\eta(q_\perp)\Lambda_2^{+}(q_\perp), \tag{B.5}$$
$$(M + \omega_1 + \omega_2)\varphi^{--} = -\Lambda_1^{-}(q_\perp)\eta(q_\perp)\Lambda_2^{-}(q_\perp). \tag{B.6}$$

From the above equations, we can see that in the weak binding condition $M \sim (\omega_1 + \omega_2)$, φ^{--} is much smaller compared with φ^{++} and can be ignored in the calculations. The normalization condition for the Salpeter wave function reads

$$\int \frac{\mathrm{d}^3 q_\perp}{(2\pi)^3}\left[\overline{\varphi}^{++}\frac{\not{P}}{M}\varphi^{++}\frac{\not{P}}{M} - \overline{\varphi}^{--}\frac{\not{P}}{M}\varphi^{--}\frac{\not{P}}{M}\right] = 2M. \tag{B.7}$$

B.2 Numerical solutions of 0^- state

Now we take the 0^- ($^1S_0$) state as an example to show the details of achieving Sapeter equations' numerical results. The Salpeter wave function for the 0^- ($^1S_0$) state has the following general form [54]:

$$\varphi(^1S_0) = M\left[k_1\frac{\not{P}}{M} + k_2 + k_3\frac{\not{q}_\perp}{M} + k_4\frac{\not{P}\not{q}_\perp}{M^2}\right]\gamma^5. \tag{B.8}$$

By utilizing the Eq. (B.4), we have the following two constraint conditions:

$$k_3 = \frac{M(\omega_1 - \omega_2)}{m_1\omega_2 + m_2\omega_1}k_2, \quad k_4 = -\frac{M(\omega_1 + \omega_2)}{m_1\omega_2 + m_2\omega_1}k_1. \tag{B.9}$$

In the above wave function, the only undetermined wave functions are k_1 and k_2, which are the functions of $q_\perp^2$.

By using the definition Eq. (B.3), we can easily get the positive Salpeter wave function of the $^1S_0$ state as Eq. (17), and the corresponding constraint conditions Eq. (18). Similarly, the Salpeter negative wave function $\varphi^{--}(^1S_0)$ is expressed as

$$\varphi^{--}(^1S_0) = \left[Z_1 + Z_2\frac{\not{P}}{M} + Z_3\frac{\not{q}_\perp}{M} + Z_4\frac{\not{P}\not{q}_\perp}{M^2}\right]\gamma^5. \tag{B.10}$$

Z_i $(i = 1, 2, 3, 4)$ has the following forms:

$$Z_1 = \frac{M}{2}\left[k_2 - \frac{\omega_1 + \omega_2}{m_1 + m_2}k_1\right], \quad Z_3 = -\frac{M(\omega_1 - \omega_2)}{m_1\omega_2 + m_2\omega_1}Z_1,$$
$$Z_2 = \frac{M}{2}\left[k_1 - \frac{m_1 + m_2}{\omega_1 + \omega_2}k_2\right], \quad Z_4 = +\frac{M(m_1 + m_2)}{m_1\omega_2 + m_2\omega_1}Z_1. \tag{B.11}$$

And now the normalization condition Eq. (B.7) becomes

$$\int \frac{\mathrm{d}^3\boldsymbol{q}}{(2\pi)^3}\frac{8M\omega_1\omega_2 k_1 k_2}{(m_1\omega_2 + m_2\omega_1)} = 1. \tag{B.12}$$

Inserting the Salpeter positive wave function of Eq. (17) and the negative wave function of Eq. (B.10) into the Salpeter equations (B.5) and (B.6), respectively, we can obtain two coupled eigenequations on k_1 and k_2 [54] as

$$\begin{cases} (M - \omega_1 - \omega_2)\left[ck_1(\boldsymbol{q}) + k_2(\boldsymbol{q})\right] = \frac{1}{2\omega_1\omega_2} \\ \quad \int \mathrm{d}^3\boldsymbol{k}\left[\beta_1 k_1(\boldsymbol{k}) + \beta_2 k_2(\boldsymbol{k})\right], \\ (M + \omega_1 + \omega_2)\left[k_2(\boldsymbol{q}) - ck_1(\boldsymbol{q})\right] = \frac{1}{2\omega_1\omega_2} \\ \quad \int \mathrm{d}^3\boldsymbol{k}\left[\beta_1 k_1(\boldsymbol{k}) - \beta_2 k_2(\boldsymbol{k})\right], \end{cases} \tag{B.13}$$

where we have used the definition $c = \frac{\omega_1 + \omega_2}{m_1 + m_2}$ and the shorthand

$$\beta_1 = \boldsymbol{k}\cdot\boldsymbol{q}(V_s + V_v)\frac{(\nu_1 + \nu_2)(\omega_1 + \omega_2)}{m_1\nu_2 + m_2\nu_1} - (V_s - V_v)(m_1\omega_2 + m_2\omega_1),$$
$$\beta_2 = \boldsymbol{k}\cdot\boldsymbol{q}(V_s + V_v)\frac{(\nu_1 - \nu_2)(m_1 - m_2)}{m_1\nu_2 + m_2\nu_1} - (V_s - V_v)(m_1 m_2 + \omega_1\omega_2 + \boldsymbol{q}^2). \tag{B.14}$$

In the above equations, V_s and V_v are the scalar and vector parts defined in Cornell potential (see Eq. (28)), respectively; we have used the definition $\nu_i = \sqrt{m_i^2 + \boldsymbol{k}^2}$ $(i = 1, 2)$.

Then by solving the two coupled eigenequations numerically, we obtain the mass spectrum and the corresponding wave functions k_1, k_2. Repeating similar procedures we can obtain the numerical wave functions for the $^1D_2$, $^3D_2$ and $^3D_3$ states. Interested reader can see more details on solving the full Salpeter equations in Refs. [34,54,55].

C Positive Salpeter wave function for $^1S_0$, $^1D_2$, and $^3D_2$

The positive Salpeter wave function and its constraint conditions for the $^1D_2$ state [40] are displayed in (C.1) and (C.2). The undetermined wave functions are f_1 and f_2. We have

$$\psi_D(^1D_2) = e_{\mu\nu}q_\perp'^{\mu}q_\perp'^{\nu}\left[b_1 + b_2\frac{\not{P}_F}{M_F} + b_3\frac{\not{q}'_\perp}{M_F} + b_4\frac{\not{P}_F\not{q}'_\perp}{M_F^2}\right]\gamma^5, \tag{C.1}$$

$$b_1 = \frac{1}{2}\left[f_1 + \frac{\omega_1' + \omega_2'}{m_1' + m_2'} f_2\right], \quad b_3 = -\frac{M_F(\omega_1' - \omega_2')}{m_1'\omega_2' + m_2'\omega_1'} b_1,$$
$$b_2 = \frac{1}{2}\left[f_2 + \frac{m_1' + m_2'}{\omega_1' + \omega_2'} f_1\right], \quad b_4 = -\frac{M_F(m_1' + m_2')}{m_1'\omega_2' + m_2'\omega_1'} b_1. \tag{C.2}$$

The positive Salpeter wave function of the $^3D_2$ state [55] and constraint conditions can be written as

$$\psi_D(^3D_2) = \mathrm{i}\epsilon_{\mu\nu\alpha\beta}\frac{P_F^\nu}{M_F} q_\perp'^\alpha e^{\beta\delta} q_{\perp\delta}' \gamma^\mu \times\left[i_1 + i_2\frac{\not{P}_F}{M_F} + i_3\frac{\not{q}_\perp'}{M_F} + i_4\frac{\not{P}_F\not{q}_\perp'}{M_F^2}\right], \tag{C.3}$$

$$i_1 = \frac{1}{2}\left[v_1 - \frac{\omega_1' + \omega_2'}{m_1' + m_2'} v_2\right], \quad i_3 = +\frac{M_F(\omega_1' - \omega_2')}{m_1'\omega_2' + m_2'\omega_1'} i_1,$$
$$i_2 = \frac{1}{2}\left[v_2 - \frac{m_1' + m_2'}{\omega_1' + \omega_2'} v_1\right], \quad i_4 = -\frac{M_F(m_1' + m_2')}{m_1'\omega_2' + m_2'\omega_1'} i_1. \tag{C.4}$$

Here we also only have two undetermined wave functions v_1 and v_2.

In Eqs. (C.1)–(C.4) the indeterminate wave functions, such as f_1 and f_2 in $\psi_D(^1D_2)$, v_1 and v_2 in $\psi_D(^3D_2)$, which are functions of $q_\perp'^2$ and can be determined numerically by solving the coupled Salpeter eigenequations (B.5) and (B.6).

References

1. P. del Amo Sanchez et al. (BABAR Collaboration), Phys. Rev. D. **82**, 111101 (2010)
2. R. Aaij et al. (LHCb Collaboration), JHEP. **09**, 145 (2013)
3. R. Aaij et al. (LHCb Collaboration), Phys. Rev. D **90**, 072003 (2014)
4. R. Aaij et al. (LHCb Collaboration), Phys. Rev. D **91**, 092002 (2015)
5. R. Aaij et al. (LHCb Collaboration), Phys. Rev. D **92**, 032002 (2015)
6. S. Godfrey, N. Isgur, Phys. Rev. D **32**, 189 (1985)
7. B. Aubert et al. (BABAR Collaboration), Phys. Rev. Lett. **97**, 222001 (2006)
8. B. Aubert et al. (BABAR Collaboration), Phys. Rev. D **80**, 092003 (2009)
9. R. Aaij et al. (LHCb Collaboration), Phys. Rev. Lett. **113**, 162001 (2014)
10. P. Colangelo, F. De Fazio, S. Nicotri, Phys. Lett. B **642**, 48 (2006)
11. P. Colangelo, F. De Fazio, F. Giannuzzi, S. Nicotri, Phys. Rev. D **86**, 054024 (2012)
12. X.-H. Zhong, Phys. Rev. D **82**, 114014 (2010)
13. Z.-F. Sun, J.-S. Yu, X. Liu, T. Matsuki, Phys. Rev. D **82**, 111501 (2010)
14. B. Chen, L. Yuan, A. Zhang, Phys. Rev. D **83**, 114025 (2011)
15. Z.-G. Wang, Phys. Rev. D **83**, 014009 (2011)
16. Q.-F. Lü, D.-M. Li, Phys. Rev. D **90**, 054024 (2014)
17. B. Chen, X. Liu, A. Zhang, Phys. Rev. D **92**, 034005 (2015)
18. G.-L. Yu, Z.-G. Wang, Z.-Y. Li, Chin. Phys. C **39**, 063101 (2015)
19. S. Godfrey, K. Moats, Phys. Rev. D **90**, 117501 (2014)
20. S. Godfrey, K. Moats, Phys. Rev. D **93**, 034035 (2016)
21. P. Colangelo, F. De Fazio, G. Nardulli, Phys. Lett. B **478**, 408 (2000)
22. L.-F. Gan, M.-Q. Huang, Phys. Rev. D **79**, 034025 (2009)
23. L.-F. Gan et al., Eur. Phys. J. C **75**, 232 (2015)
24. T.B. Suzuki, T. Ito, S. Sawada, M. Matsuda, Prog. Theor. Phys. **91**, 757 (1994)
25. S. Veseli, M.G. Olsson, Phys. Rev. D **54**, 886 (1996)
26. J.P. Lees et al. (BaBar Collaboration), Phys. Rev. Lett. **109**, 101802 (2012)
27. S. Hirose et al. (Belle Collaboration). arXiv:1612.00529 [hep-ex]
28. S. Fajfer, J.F. Kamenik, I. Nišandžić, Phys. Rev. D **85**, 094025 (2012)
29. M. Tanaka, R. Watanabe, Phys. Rev. D **87**, 034028 (2013)
30. Y.-Y. Fan, Z.-J. Xiao, R.-M. Wang, B.-Z. Li, Sci. Bull. **60**, 2009 (2015)
31. E.E. Salpeter, Phys. Rev. **87**, 328 (1952)
32. E. Salpeter, H. Bethe, Phys. Rev. **84**, 1232 (1951)
33. Z. Wang, G.-L. Wang, C.-H. Chang, J. Phys. G Nucl. Part. Phys. **39**, 015009 (2012)
34. T. Wang, G.-L. Wang, Y. Jiang, W.-L. Ju, J. Phys. G. Nucl. Part. Phys. **40**, 035003 (2013). doi:10.1088/0954-3899/40/3/035003
35. W.-L. Ju, G.-L. Wang, H.-F. Fu, Z.-H. Wang, Y. Li, JHEP **09**, 171 (2015)
36. Q. Li, T. Wang, Y. Jiang et al., Eur. Phys. J. C **76**, 454 (2016). doi:10.1140/epjc/s10052-016-4306-3
37. G.-L. Wang, Phys. Lett. B **633**, 492 (2006)
38. G.-L. Wang, Phys. Lett. B **650**, 15 (2007)
39. G.-L. Wang, Phys. Lett. B **674**, 172 (2009)
40. T. Wang, G.-L. Wang, W.-L. Ju, Y. Jiang, JHEP **03**, 110 (2013)
41. D. Fakirov, B. Stech, Nucl. Phys. B **133**, 315 (1978)
42. N. Cabibbo, L. Maiani, Phys. Lett. B **73**, 418 (1978)
43. M. Bauer, B. Stech, M. Wirbel, Z. Phys. C **34**, 103 (1987)
44. A. Ali, G. Kramer, C.D. Lu, Phys. Rev. D **58**, 094009 (1998)
45. C.-H. Chang, Y.-Q. Chen, Phys. Rev. D **49**, 3399 (1994)
46. P. Colangelo, F. De Fazio, Phys. Rev. D **61**, 034012 (2000). doi:10.1103/PhysRevD.61.034012. arXiv:hep-ph/9909423
47. M.A. Ivanov, J.G. Körner, P. Santorelli, Phys. Rev. D **73**, 054024 (2006)
48. E. Hernández, J. Nieves, J.M. Verde-Velasco, Phys. Rev. D **74**, 074008 (2006)
49. R.N. Faustov, V.O. Galkin, Phys. Rev. D **87**, 034033 (2013)
50. M.J. Dugan, B. Grinstein, Phys. Lett. B **255**, 583 (1991)
51. M. Beneke, G. Buchalla, M. Neubert, C.T. Sachrajda, Phys. Rev. Lett. **83**, 1914 (1999). doi:10.1103/PhysRevLett.83.1914. arXiv:hep-ph/9905312
52. Y. Y. Keum, H.N. Li, Phys. Rev. D **63**, 074006 (2001). doi:10.1103/PhysRevD.63.074006. arXiv:hep-ph/0006001
53. S. Mandelstam, Proc. Roy. Soc. A **233**, 248 (1955)
54. C.S. Kim, G.-L. Wang, Phys. Lett. B **584**, 285 (2004)
55. T. Wang, H.-F. Fu, Y. Jiang, Q. Li, G.-L. Wang. arXiv:1601.01047 [hep-ph]
56. L. Bergström, H. Grotch, R.W. Robinett, Phys. Rev. D. **43**, 7 (1991)
57. T. Matsuki, T. Morii, K. Seo, Prog. Theor. Phys. **124**, 2 (2010)
58. D. Ebert, R.N. Faustov, V.O. Galkin, Eur. Phys. J. C **66**, 197 (2010)
59. K.A. Olive et al. (Particle Data Group), Chin. Phys. C **38**, 090001 (2014)
60. N. Devlani, V.H. Kher, A.K. Rai, EPJ. Web. Conf. **95**, 05006 (2015)
61. N. Devlani, A.K. Rai, Eur. Phys. J. A **48**, 104 (2012)